Mitochondrial genome copy number measured by DNA sequencing in human blood is strongly associated with metabolic traits via cell-type composition differences

Liron Ganel,[1,2] Lei Chen,[1,2] Ryan Christ,[1] Jagadish Vangipurapu,[3] Erica Young,[1,4] Indraniel Das,[1] Krishna Kanchi,[1] David Larson,[1,5] Allison Regier,[1,2] Haley Abel,[1,2,5] Chul Joo Kang,[1] Alexandra Scott,[1,2] Aki Havulinna,[6,7] Charleston W. K. Chiang,[8,9] Susan Service,[10] Nelson Freimer,[10] Aarno Palotie,[6,11,12] Samuli Ripatti,[6,12,13] Johanna Kuusisto,[3,14] Michael Boehnke,[15] Markku Laakso,[3,14] Adam Locke,[1,2] Nathan O. Stitziel,[1,4,5]* Ira M. Hall,[1,2,16]*

[1] McDonnell Genome Institute, Washington University School of Medicine, St. Louis, MO, United States of America

[2] Department of Medicine, Washington University School of Medicine, St. Louis, MO, United States of America

[3] Institute of Clinical Medicine, Internal Medicine, University of Eastern Finland, Kuopio, Finland

[4] Department of Medicine, Cardiovascular Division, Washington University School of Medicine, St. Louis, MO, United States of America

[5] Department of Genetics, Washington University School of Medicine, St. Louis, MO, United States of America

[6] Institute for Molecular Medicine Finland (FIMM), HiLIFE, University of Helsinki, Helsinki, Finland

[7] Finnish Institute for Health and Welfare (THL), Helsinki, Finland

[8] Center for Genetic Epidemiology, Department of Preventive Medicine, Keck School of Medicine, University of Southern California, Los Angeles, CA, United States of America

[9] Quantitative and Computational Biology Section, Department of Biological Sciences, University of Southern California, Los Angeles, CA, United States of America

[10] Center for Neurobehavioral Genetics, Jane and Terry Semel Institute for Neuroscience and Human Behavior, University of California Los Angeles, Los Angeles, CA, United States of America

[11] Analytical and Translational Genetics Unit (ATGU), Psychiatric & Neurodevelopmental Genetics Unit, Departments of Psychiatry and Neurology, Massachusetts General Hospital, Boston, MA, United States of America

[12] Broad Institute of MIT and Harvard, Cambridge, MA, United States of America

[13] Faculty of Medicine, University of Helsinki, Helsinki, Finland

[14] Department of Medicine, Kuopio University Hospital, Kuopio, Finland

[15] Department of Biostatistics and Center for Statistical Genetics, University of Michigan School of Public Health, Ann Arbor, MI, United States of America

[16] Department of Genetics, Yale University School of Medicine, New Haven, CT, United States of America

* Correspondence: ira.hall@yale.edu (I.M.H.), nstitziel@wustl.edu (N.O.S.)

Abstract

Mitochondrial genome copy number (MT-CN) varies among humans and across tissues and is highly heritable, but its causes and consequences are not well understood. When measured by bulk DNA sequencing in blood, MT-CN may reflect a combination of the number of mitochondria per cell and cell type composition. Here, we studied MT-CN variation in blood-derived DNA from 19,184 Finnish individuals using a combination of genome (N = 4,163) and exome sequencing (N = 19,034) data as well as imputed genotypes (N = 17,718). We identified two loci significantly associated with MT-CN variation: a common variant at the *MYB-HBS1L* locus ($P = 1.6\times10^{-8}$), which has previously been associated with numerous hematological parameters; and a burden of rare variants in the *TMBIM1* gene ($P = 3.0\times10^{-8}$), which has been reported to protect against non-alcoholic fatty liver disease. We also found that MT-CN is strongly associated with insulin levels ($P = 2.0\times10^{-21}$) and other metabolic syndrome (metS) related traits. Using a Mendelian randomization framework, we show evidence that MT-CN measured in blood is causally related to insulin levels. We then applied an MT-CN polygenic risk score (PRS) derived from Finnish data to the UK Biobank, where the association between the PRS and metS traits was replicated. Adjusting for cell counts largely eliminated these signals, suggesting that MT-CN affects metS via cell type composition. These results suggest that measurements of MT-CN in blood-derived DNA partially reflect differences in cell-type composition and that these differences are causally linked to insulin and related traits.

Introduction

There are many reported links between mitochondrial content and cardiometabolic phenotypes in various tissues, including adipose[1–3], liver[1,4,5], skeletal muscle[1,6–10], and blood[11–17]. Traits associated

with mitochondrial (MT) content include coronary heart disease (CHD), type 2 diabetes, and metabolic syndrome traits such as insulin sensitivity/resistance, obesity, and blood triglycerides. However, these studies have generally been limited by small sample sizes and low statistical power. This, in addition to the use of heterogeneous mitochondrial quantification methods[18], has led to inconsistencies in the literature about the strength and directions of effect between mitochondrial content and metabolic syndrome (metS) traits. In one large WGS study of mitochondrial genome copy number (MT-CN) in 2,077 Sardinians, Ding *et al*. estimated the heritability of MT-CN at 54% and detected significant associations between MT-CN and both waist circumference and waist-hip ratio, but found no association with body mass index (BMI)[11]. Another large study (N = 5,150) found virtually no evidence of association between qPCR-measured MT-CN and any of several cardiometabolic phenotypes[19]. The only exception was an inverse association with insulin that was identified in one cohort but did not survive meta-analysis across cohorts. However, a study of 21,870 individuals from 3 cohorts showed a significant inverse relationship between MT-CN (measured by microarray probe intensities in two cohorts and qPCR in the third) and incident cardiovascular disease[20].

Although variations in MT-CN measured from whole blood can in principle be attributed to either variability of MT copy number within cells or the cell type composition of the blood (given that different cell types have varying MT content[21–23]), the literature on this subject is inconclusive. Using CpG methylation data, a large (N = 11,443), low-coverage (1.7x autosomal; 102x mitochondrial) sequencing study of the link between MT-CN and major depressive disorder using buccal DNA from Chinese women concluded that variability of MT-CN from buccal swabs was not due to differences in cell type composition[24]. However, this study did not do a similar experiment in blood. Two small (N = 756 and N = 400) studies identified an association between MT content and CHD that they attributed to variable MT-CN within leukocytes, but they did not directly investigate the possibility of cell type

85 composition being the true driver of the association[12,17]. For brevity, we will use the term “MT-CN” to
86 refer to the underlying phenotype reflected by measuring this quantity for the remainder of this work,
87 with these caveats.

88 While several studies have found that peripheral blood MT content is heritable, only a small
89 number of MT-CN associated loci have been identified[25–27]. In one of these studies, Curran *et al*. used
90 linkage analysis in Mexican Americans to find an MT-CN associated locus near a marker previously
91 associated with triglyceride levels[26,28,29], providing further indirect evidence for the link between
92 MT-CN and metabolic syndrome.

93 Here, we take advantage of large-scale genome, exome, and array genotype data to
94 investigate the causes and effects of MT-CN in a large, deeply phenotyped Finnish cohort. Our
95 results reveal novel links with metabolic syndrome and provide evidence supporting a causal role for
96 MT-CN.

97

98 ## Material and Methods

99 ### Genotype and phenotype data

100 Whole genome sequencing (WGS) was performed on a cohort of 4,163 samples comprising 3,074
101 male samples from the METSIM study[30] and 1,089 male and female samples from the FINRISK
102 study[31]. Genomic DNA was fragmented on the Covaris LE220 instrument targeting 375 bp inserts.
103 Automated Illumina libraries were constructed with the TruSeq PCR-free (Illumina) or KAPA Hyper
104 PCR-free library prep kit (KAPA Biosystems/Roche) on the SciClone NGS platform (Perkin Elmer).
105 The fragmented genomic DNA was size-selected on the SciClone instrument with AMPure XP beads
106 to tighten the distribution of fragmented DNA to ensure the average insert of the libraries was
107 350-375 bp. We followed the manufacturer’s protocol as provided by Perkin Elmer, with the following
108 exception: post ligation, the libraries were purified twice with a 0.7x AMPure bead/sample ratio to

eliminate any residual adaptors present. An aliquot of the final libraries was diluted 1:20 and quantitated on the Caliper GX instrument (Perkin Elmer). The concentration of each library was accurately determined through qPCR utilizing the KAPA library Quantification Kit according to the manufacturer's protocol (KAPA Biosystems/Roche) to produce cluster counts appropriate for the Illumina HiSeqX instrument. Libraries were pooled and run over a few lanes of the HiSeq X to ensure the libraries within the pool were equally balanced. The final pool of balanced libraries was loaded over the remaining number of HiSeq X lanes to achieve the desired coverage for this project. 2x150 paired end sequence data were demultiplexed using a single index, which was a restriction on the HiSeqX instrument at this time. A minimum of 19.5x coverage was achieved per sample.

The quality of the aligned sequence data was assessed using metrics generated by Picard[32] v2.4.1, Samtools[33] v1.3.1 and VerifyBamID[34] v1.1.3. Based on the output files from Picard, the following alignment statistics were collected for review: PF_MISMATCH_RATE, PF_READS, PF_ALIGNED_BASES, PCT_ADAPTER, PCT_CHIMERAS, PCT_PF_READS_ALIGNED, PCT_READS_ALIGNED_IN_PAIRS, PF_HQ_ALIGNED_BASES, PF_HQ_ALIGNED_Q20_BASES, PF_HQ_ALIGNED_READS, MEAN_INSERT_SIZE, STANDARD_DEVIATION, MEDIAN_INSERT_SIZE, TOTAL_READS, PCT_10x, and PCT_20x. Alignment rate was calculated as PF_READS_ALIGNED/TOTAL_READS. The formula for haploid coverage was as follows: $Haploid\ coverage = MEAN_COVERAGE * \frac{1-PCT_EXC_DUPE}{1-PCT_EXC_TOTAL}$. From the Samtools output, inter-chromosomal rate was calculated as: $\frac{reads_mapped_in_interchromosomal_pairs}{reads_mapped_in_pair}$ and discordant rate was calculated as: $reads_mapped_percentage - reads_mapped_in_proper_pairs_percentage$. Properly paired percentage (reads_mapped_in_proper_pairs_percentage) and singleton percentage (reads_mapped_as_singleton_percentage) were also reviewed. From VerifyBamID, the Freemix value was reviewed.

The metrics for judgement of passing data quality were: FIRST_OF_PAIR_MISMATCH_RATE < .05, SECOND_OF_PAIR_MISMATCH_RATE < 0.05, haploid coverage ≥ 19.5, interchromosomal rate < .05, and discordant rate < 5. All of the above metrics must have been met in order for the sample to be assigned as QC pass. If a sample did not meet the passing criteria, the following failure analysis was performed: a) If the Freemix score was at least 0.05, the sample or the library was considered contaminated, and both the library and the sample were abandoned; b) if the discordant rate was over 5 and/or the inter-chromosomal rate was over 0.05, the quality of DNA was considered poor and the sample was removed from the sequencing pipeline; and c) in the case of a) and b), the collaborator was contacted to determine if selection of a replacement sample from the same cohort was desired or feasible.

Separately, whole exome sequencing (WES) data (N = 19,034), genotyping array data (N = 17,718) imputed using the Haplotype Reference Consortium panel[35] v1.1, and transformed, normalized quantitative cardiometabolic trait data were obtained from an earlier study[36]. FINRISK array data came in nine genotyping batches, two of which were excluded from the present study due to small sample size. The traits, normalization and transformation procedures, and sample sizes are described in a previous publication[36]. The WES and imputed sample sets contained 4,013 and 3,929 of the 4,163 WGS samples included in the present study.

All participants in both the METSIM and FINRISK studies provided informed consent, and study protocols were approved by the Ethics Committees at participating institutions (National Public Health Institute of Finland; Hospital District of Helsinki and Uusimaa; Hospital District of Northern Savo). All relevant ethics committees approved this study.

WGS callset generation and quality control

Single nucleotide polymorphisms (SNPs) and small insertions and deletions were called from the full set of 4,163 samples using GATK[37] v3.5. GVCFs containing SNVs and Indels from GATK HaplotypeCaller (`-ERC GVCF -GQB 5 -GQB 20 -GQB 60 -variant_index_type LINEAR -variant_index_parameter 128000`) were first processed to ensure no GVCF blocks crossed boundaries every 1 Mb (CombineGVCFs; `--breakBandsAtMultiplesOf 1000000`). The resulting GVCFs were then processed in 10 Mb shards across each chromosome. Each shard was combined (CombineGVCFs), genotyped (GenotypeGVCFs; `-stand_call_conf 30 -stand_emit_conf 0`), hard filtered to remove alternate alleles uncalled in any individual removed (SelectVariants; `--removeUnusedAlternates`), and hard filtered to remove lines solely reporting symbolic deletions in parallel. All shards were jointly recalibrated (VariantRecalibrator) and then individually filtered (ApplyRecalibration) based on the recalibration results. All of the above methods were performed using GATK v3.5. SNP variant recalibration was performed using the following options to VariantRecalibrator and all resources were drawn from the GATK hg38 resource bundle (v0):

```
-mode SNP
-resource:hapmap,known=false,training=true,truth=true,prior=15.0
-resource:omni,known=false,training=true,truth=true,prior=12.0
-resource:1000G,known=false,training=true,truth=false,prior=10.0
-resource:dbsnp,known=true,training=false,truth=false,prior=2.0
-an QD -an DP -an FS -an MQRankSum -an ReadPosRankSum
-tranche 100.0 -tranche 99.9 -tranche 99.0 -tranche 90.0
```

Indel variant recalibration was performed using the following options to VariantRecalibrator (with the same resource bundle as with SNPs):

```
-mode INDEL
```

```
-resource:mills,known=true,training=true,truth=true,prior=12.0
-an DP -an FS -an MQRankSum -an ReadPosRankSum
--maxGaussians 4
-tranche 100.0 -tranche 99.9 -tranche 99.0 -tranche 90.0
```

When applying the variant recalibration the following options were used:

For SNPs: `--ts_filter_level 99.0`

For Indels: `--ts_filter_level 99.0`

Following SNP and INDEL variant recalibration, multiallelic variants were decomposed and normalized with vt[38] v0.5. Duplicate variants and variants with symbolic alleles were subsequently removed. The bottom tranche of variants identified by GATK's Variant Quality Score Recalibration tool and variants with missingness greater than 2% were removed as well, although variants with allele balance between 0.3 and 0.7 were rescued. Variants with Hardy-Weinberg equilibrium (on a second-degree unrelated subset of 3,969 individuals, as determined by KING[39]) P value less than 10^{-6} and those with allele balance less than 0.3 or greater than 0.7 were also removed.

Sample-level quality control was also undertaken on this dataset; 13 samples were identified for exclusion because of singleton counts that were at least eight median absolute deviations above the median. Separately, 12 sex-discordant samples were flagged using `plink --check-sex`, and after examining chromosome Y missingness and F coefficient values for these samples, only the one that clearly differed from its reported sex was marked for exclusion. No samples were excluded based on missingness fraction or the first five principal components. In total, 14 samples were excluded from the heritability, GWAS, and Mendelian randomization analyses; the other analyses were performed without exclusion of these samples. As a result, the former analyses were performed with N = 4,149 while the latter had N = 4,163.

203

204 **Mitochondrial genome copy number estimation**

205 We estimated mitochondrial genome copy number (MT-CN) from both WGS and WES data. In WGS
206 data, we used BEDTools[40] to calculate per-base coverage on the mitochondrial genome from the
207 latest available 4,163 WGS CRAM files. MT-CN was then calculated by normalizing the mean
208 coverage of the mitochondrial genome to the "haploid coverage" of the autosomes as calculated by
209 Picard[32]. The result was then doubled to account for the diploidy of the autosomal genome. This
210 normalization is summarized by the following equation: $MT_CN_{WGS} = 2 \times \frac{mean\ mtDNA\ coverage}{haploid\ autosomal\ coverage}$.

211 The output from the above equation served as the raw measurement of per sample MT-CN. To
212 reduce batch effects, we separated the 4,163 samples into three groups: METSIM, FINRISK collected
213 in 1992 or 1997, and FINRISK collected in 2002 or 2007 (the FINRISK batching decisions were made
214 based on the means shown in **Figure S4**). Within each cohort, the raw estimates were regressed on
215 age, age^2 and sex (FINRISK only) and the residuals were inverse-normal transformed. We combined
216 the three batches of normalized MT-CN values and inverse-normal transformed the combined values
217 for downstream analysis.

218 We used a similar procedure to estimate MT-CN from WES data, with mean autosomal
219 coverage estimates taken from XHMM[41]. However, as mitochondrial genomic coverage was
220 nonuniform due to the use of hybrid capture probes, mean mtDNA coverage was not an obvious
221 choice of metric for MT-CN estimation (**Figure S5**). To summarize this nonuniform mitochondrial
222 genomic coverage into a single number, we tried taking the mean and the maximum depth of reads
223 that aligned to the mitochondrial chromosome; the resulting values were then processed in the same
224 way as the WGS-estimated values. We evaluated the approaches by measuring the R^2 between
225 WGS-estimated and WES-estimated MT-CN in the 4,013 samples for which both data types were
226 available (**Figure S6**). While R^2 was fairly high using both approaches, the maximum coverage

227 method was ultimately selected for use as it yielded a higher R^2 (0.445 vs 0.380). As a result, the
228 WES MT-CN estimate was calculated as follows: $MT_CN_{WES} = 2 \times \frac{maximum\ mtDNA\ coverage}{mean\ haploid\ autosomal\ coverage}$.

229

230 **Mitochondrial haplogroup estimation**

231 We assigned mitochondrial haplogroups using HaploGrep[42] v1.0. Mitochondrial SNP/indel variants
232 were genotyped using GATK GenotypeGVCFs, and a customized filter based on allele balance was
233 applied to the combined callset. HaploGrep was then used to call mitochondrial haplotypes for each
234 individual. We adjusted for major haplogroups in the same linear regressions of metabolic traits onto
235 MT-CN (see Results) and calculated the summary statistics from a permutation test as implemented
236 in the R package lmPerm.

237

238 **Heritability analysis**

239 To estimate heritability of MT-CN, a genomic relatedness-based restricted maximum-likelihood
240 (GREML) method was used as implemented in GCTA[43]. The original GREML[44] method was used first,
241 followed by GREML-LDMS[45] to account for biases arising from differences in minor allele frequency
242 (MAF) spectrum or linkage disequilibrium (LD) properties between the genotyped variants and the
243 true causal variants[46]. For both analyses, MT-CN values were normalized and residualized for sex,
244 age, and age^2 as described above. Heritability estimation was performed jointly and separately for
245 METSIM and FINRISK samples using WGS and imputed array genotypes. In all cases, a minimum
246 MAF threshold of 1% was applied. Beyond those covariates already adjusted for in the normalization
247 process, sensitivity analyses were performed on imputed array data to determine whether heritability
248 estimates were sensitive to inclusion of covariates. In these experiments, either cohort or FINRISK
249 genotyping array batch were included as fixed-effect covariates in joint analyses of imputed array
250 data; in neither case was the final heritability estimate significantly affected (h^2 = 0.09, SE = 0.02 in

251 both cases). In GREML-LDMS, genotypes were split into four SNP-based LD score quartiles and two
252 MAF bins (1% > MAF > 5% and MAF > 5%), and genetic relatedness matrices (GRMs) were
253 estimated separately for each of the eight combinations. The GREML algorithm was then run on all
254 eight GRMs simultaneously using the first ten principal components (PCs) of the genotype matrix (as
255 calculated by smartPCA v13050) as fixed covariates[45]. The use of GREML-LDMS over GREML also
256 did not affect estimated heritability values (**Table 3**), suggesting that the properties of the causal
257 variants for this trait do not lead to significant biases when using the standard GREML approach.

258 We observed that WGS heritability estimates decrease when analyzing FINRISK and METSIM
259 data together compared to analysis of METSIM alone (**Table 2**) (note that FINRISK-only heritability
260 estimates are not reliable as they have large standard errors resulting from the small number of
261 FINRISK samples sequenced). One potential explanation for this is that there exists substantial
262 heterogeneity across FINRISK survey years (**Figure S4**), and between the FINRISK and METSIM
263 cohorts, with respect to the reliability with which mtDNA was captured (likely due to different DNA
264 preparation protocols).

265

266 **Genome-wide association analyses**

267 Genome-wide association studies (GWAS) were performed using the same normalized phenotype
268 used in heritability analyses. Single-variant GWAS were conducted using EMMAX as implemented in
269 EPACTS. Kinship matrices required by EMMAX were generated by EPACTS; kinship matrices for
270 WGS GWAS were generated from WGS data, while those for WES and imputed array based GWAS
271 were generated from WES data. A P value threshold of 5×10^{-8} was used for the WGS and imputed
272 array GWAS while 5×10^{-7} was used for significance in the WES GWAS. Single-variant association
273 analyses of WGS and WES data did not include any covariates in the EMMAX model, although all
274 association analyses were performed using MT-CN values that adjusted for age, age^2, sex, and

275 cohort (see “Mitochondrial Genome Copy Number Estimation”). All association tests labeled “joint”
276 were performed on METSIM and FINRISK cohorts together; in one case, a random-effects
277 meta-analysis was performed using individual-cohort summary statistics and the R package meta[47].

278 Gene-based variant aggregation studies (RVAS) were done using a mixed-model version of
279 SKAT-O[48] as implemented in EPACTS. Variants with CADD[49] score greater than 20 and minor allele
280 frequency less than 1% were grouped into genes as annotated by VEP[50] (which annotates a variant
281 with a gene name if the gene falls within 5k of that gene by default). For gene-based RVAS,
282 genome-wide significance thresholds varied slightly due to differing the number of genes with at least
283 two variants meeting the above criteria in each test, but were approximately 2×10^{-6} in all cases.

284

285 **Mendelian randomization**

286 To assess the evidence for a causal relationship between mitochondrial genome copy number and
287 fasting serum insulin levels, the METSIM cohort alone was used due to its homogeneity of sex,
288 collection procedures, and location. A penalized regression based, multiple variant Mendelian
289 randomization (MR) approach was employed to enforce the necessary assumptions of MR methods.
290 While some MR studies have tested one or more assumptions *post hoc*, to our knowledge, there is no
291 published method that tries to enforce these assumptions during the process of building the genetic
292 instrument in the absence of a large set of known genotype-exposure associations. In our formulation
293 (**Figure 4a**), X, the natural log of MT-CN (adjusted for nuclear genomic coverage but not for age,
294 age^2, or sex), and a genotype matrix G were used to build a genetic instrument Z, which was then
295 tested against Y, the natural log of fasting serum insulin. The goal of the MR approach was to use a
296 large number of common variants to build a genetic instrument Z that satisfied the three assumptions
297 of MR[51]:

298 1. Association of Z with X

2. Independence of Z from any variables U confounding the relationship between X and Y
3. Independence of Z and Y given X and U

To attempt to build a genetic instrument satisfying assumptions 2 and 3, the deep METSIM phenotype data were leveraged. A matrix W was constructed using the 75 measured traits and first 20 PCs of the genotype matrix (including a third-degree polynomial basis for PC 1). From these variables, covariates that could violate one of these two assumptions were chosen by selecting columns of W associated with X or Y (**Figure 4b**). These columns were selected using two successive LASSO feature selection procedures. First, a set A of covariates associated with Y was chosen by using LASSO to regress Y onto W. In this regression, age and the third-degree polynomial basis for PC 1 were left unpenalized to ensure that A contains these covariates. The shrinkage parameter was chosen by tenfold cross-validation as the largest value that gives a mean squared error (MSE) within one standard error of the minimum observed MSE. Next, the columns of W associated with X conditional on A were chosen using a similar LASSO procedure in the regression of X onto W. In this step, however, the variables in set A were left unpenalized in order to only capture associations that are conditionally independent of A. The selected variables from this regression were designated set B.

The instrument was built using a penalized regression (using either an L1 or L2 penalty, as implemented in glmnet[52]) of the form $X \sim G + W_A + W_B$, where W_A and W_B are the columns of W representing sets A and B, respectively, and G is a genotype matrix containing the alternate allele dosage (missing alleles are replaced with the MAF, similarly to PLINK[53]) of all variants with MAF greater than 1% and marginal GWAS P value below 0.01. As X was the target vector for this regression, assumption 1 of MR was trivial. In the penalized regression, W_A and W_B were unpenalized in an effort to orthogonalize the regression coefficients of the genotypes to these covariates in an effort to enforce assumptions 2 and 3. glmnet was run with a convergence threshold of 1×10^{-10} and

maximum number of iterations of 200,000. To avoid the overfitting that would result from calculating instrument values on the same samples on which regression coefficients are learned[54], the penalized regression model was fit on independent subsets of the data as follows. Five models were fit, each by holding out a different 20% of samples, such that the instrument value computed for each sample was calculated using the regression coefficient vector learned without that sample. The vector of possible shrinkage parameters λ for all five models was supplied as ($10^3, 10^2, \ldots, 10^{-13}, 10^{-14}$), and the λ value which minimized the joint residual sum of squares of all five models was chosen for instrument calculation.

Formally, we randomly partitioned the set of samples S with nonmissing insulin measurements into five nonoverlapping sets S_j for $j = \{1, \ldots, 5\}$. We denote set complements as $S_j^C = S \setminus S_j$, such that each S_j^C contained 80% of the training samples. The instrument vector Z_j for each S_j was computed as follows: $Z_j = G_j \times \beta_G^{(-j)}$, where Z_j is the instrument vector for S_j, G_j is the genotype matrix of S_j, and $\beta_G^{(-j)}$ is the vector of genotype regression coefficients from the model described above, trained on S_j^C. The instrument values within each S_j were inverse rank-normalized using a Blom transformation[55,56] before being concatenated across the values of j to give the final instrument vector Z. Because samples with missing insulin values could not be included in the causality test anyway, these samples were excluded from S but safely included in the training sets of all five models. The instrument values of these samples were never calculated or used in downstream analyses.

Often, the inclusion of unpenalized covariate sets A and B in the instrument-building regression was not sufficient to completely orthogonalize Z to these covariates (see below). As a result, the test for association between Z and Y was performed conditional on a set of potentially assumption-violating covariates chosen using the newly constructed instrument Z in another attempt to account for possible violations of MR assumptions in the causality test (**Figure 4c**). To choose this set of covariates C, a final feature selection step was performed using LASSO regression of Z on W

with covariate set A excluded from the penalty. As in the previous feature selection steps, the shrinkage parameter was chosen via tenfold cross-validation as the largest value with MSE within one standard error of the minimum observed MSE. Once this set, D, of covariates associated with Z was chosen, the covariates in W were partitioned into sets I, II, III, and IV based on their membership in A and D (see **Figure 4**). Formally, this partitioning was done as follows: $I = W \setminus (A \cup D)$, $II = D \cap A^C$, $III = A \cap D^C$, and $IV = A \cap D$, where $A^C = W \setminus A$ and $D^C = W \setminus D$. Then, the test for causality came from the regression coefficient of Z in the multiple regression $Y \sim Z + C$, where C is the union of sets II, III, and IV (colored blue in **Figure 4c**).

To account for missing data in W, missing values were multiply imputed using regression trees as implemented in the R package mice[57] v3.4.0 (`maxit=25`). This imputation was repeated 1000 times in parallel, with each set of imputed values being carried through the entire procedure described above. The resulting 1000 computed instrument effect sizes and standard errors were combined using Rubin's method as implemented in the R package Amelia[58] v1.7.5. The combined effect size and standard error were then tested for significance using a t-test with 998 degrees of freedom.

The above procedure was performed separately for METSIM samples with WGS data (N = 3,034) and METSIM samples with only imputed array data (N = 6,774) using an L1 penalty in the instrument-building regression, and again using an L2 penalty. Both sample sets were limited to those for which relevant quantitative traits were available. An inverse-variance weighted meta-analysis was performed across data sets for L1 and L2-penalized regression separately. The resulting effect size and standard error were tested for significance using a Z test.

To ensure that our results were not driven by outlier samples, we removed outliers in two stages. Before the MR analyses, we used principal components analysis (PCA), Mahalanobis distance, and multi-trait extreme outlier identification to remove 5 WGS samples and 15 imputed

array samples based on quantitative trait data. We also removed high leverage, high residual outliers from the causality test regression (see below) *post hoc* and recomputed the instrument effect sizes to ensure that there was no significant change in the results. In each of the 1,000 multiple imputation runs, among the samples with standardized residual greater than 1, the top 10 samples by leverage were recorded. Any sample that was recorded in this way in at least one run was then excluded from the re-analysis as a *post hoc* outlier. The results of this additional analysis showed only very small differences in effect estimates, and their interpretation remained the same (**Table S9**). Thus, we concluded that our causal inference results were not driven by outlier samples.

One caveat of this method is that, as mentioned above, exclusion of sets A and B from the regression penalty did not perfectly orthogonalize the resulting instrument from these variables in practice (**Figure S7**). Reasons for this may include relatively low levels of shrinkage in the instrument-building regression or higher order associations between MT-CN and the confounding variables. However, our method still represents an improvement over the current standard, which is not to adjust for these covariates at all. Another caveat is that it is impossible to determine the perfect set of covariates for which adjustment is appropriate. Lack of adjustment for truly confounding variables can result in an instrument which does not satisfy MR assumptions 2 and/or 3, yielding a biased effect estimate. Conversely, unnecessary adjustment for certain variables can also result in biases. For example, adjusting for an intermediate phenotype that truly lies along the path from Z to X to Y can cause a false negative signal, making the causality test overly conservative. Alternatively, adjusting for some variables can result in collider biases[59]. That is, if both Z and Y are causal for a confounder U, then adjusting for U can induce a dependency between Z and Y (**Figure S8**) that did not previously exist.

We note that a known source of bias in MR studies is the selection of samples based on case-control status for a related disease[60]. While METSIM is a population-based study, samples were

395 selected for WGS based on cardiovascular disease case-control status so as to enrich the sequenced
396 samples for cases. This has the potential to bias a MR experiment if both the exposure and the
397 outcome are associated with the disease, which is certainly possible. However, in our design, all of
398 the METSIM samples not chosen for WGS were tested in the imputed array experiment. The
399 consistency of effect estimates between the WGS and imputed array samples both in the L1 and L2
400 penalty cases (**Figure 4d**) suggests that there is little to no bias arising from sample selection in this
401 experiment.
402

403 **Calculation and testing of polygenic risk score in the UK Biobank**

404 To search for associations between MT-CN and other phenotypes, the genetic instrument calculated
405 in Finnish imputed array data was computed and treated as a polygenic risk score (PRS) in a
406 relatively homogenous subset of 357,656 UK Biobank samples identified by a previous study[61]. We
407 calculated $\overline{\beta_G}$, the average of the five values of $\beta_G^{(-j)}$ across all 1000 multiple imputation runs using an
408 L2 penalty and imputed array data – the L2 penalty was chosen because it performed better than the
409 L1 on both METSIM data types, and the imputed array data set was chosen due to its larger sample
410 size than the WGS set (**Figure 4d**). Next, to keep the procedure as consistent as possible with the
411 imputation protocol used for METSIM – which used haploid dosage values to call imputed
412 genotypes[36] – we called imputed genotypes using the expected alternate allele dosage from the UK
413 Biobank by setting thresholds of 0.5 and 1.5. Using the resulting imputed variant calls, we calculated
414 our PRS as $\tilde{Z} = \overline{\beta_G} \times \tilde{G}$, where $\tilde{G}$ is the UK Biobank genotype dosage matrix constructed in the
415 same way as G in METSIM.

416 To test for associations with MT-CN PRS in the UK Biobank, we employed two approaches: a
417 hypothesis-driven analysis targeted to the phenotypes associated with MT-CN in the Finnish data as
418 well as a hypothesis-free screen of all the phenotypes available to us.

419 In the targeted analysis, we used our genetic instrument from the MR experiment as a PRS for
420 MT-CN in our chosen subset of the UK Biobank and tested for associations with several blood cell
421 count and metabolic syndrome traits. Given the association of MT-CN with rs9389268 (see Results),
422 we selected as cell count traits total leukocyte count as well as lymphocyte, neutrophil, monocyte,
423 and platelet counts for testing (because lymphocyte count was not readily available, it was calculated
424 as the product of leukocyte count and lymphocyte percentage). We did not include basophils and
425 eosinophils in this analysis considering that they comprise a small minority of white blood cells and
426 are unlikely to affect MT-CN measured from whole blood. All cell count traits were log-transformed
427 and standardized separately by sex.

428 We took several steps to eliminate outlier samples in the dataset. Through three iterations of
429 PCA on the cell count matrix and subsequent outlier removal, we removed 1,637 outlier samples. We
430 then fit null linear models of the form $cell\ count \sim age + age^2 + sex + age : sex + age^2 : sex + PCs$ (the first
431 20 PCs were included) for each cell count trait and subsequently removed samples with either large
432 residuals or high leverage and moderate residuals in at least one model (following the example of [61]).
433 Through two iterations of null model fitting and outlier removal, we removed 7 additional samples
434 based on null model fit. Tests of association between cell counts and MT-CN PRS were based on the
435 PRS regression coefficient in linear models of the form
436 $cell\ count \sim PRS + age + age^2 + sex + age : sex + age^2 : sex + PCs$.

437 We repeated this process for those cardiometabolic traits found to be suggestively associated
438 with MT-CN in the Finnish dataset ($P < 10^{-6}$) that were also readily available in the UK Biobank
439 (**Figure 1a**, **Table S1**); these phenotypes were body mass index (BMI), fat mass, C-reactive protein,
440 high-density lipoprotein, total triglycerides, and weight. We also chose to include T2D status because
441 of the lack of insulin measurement in the UK Biobank. Except for T2D, a binary trait, all traits were
442 log-transformed before further analysis (after removing 817 samples with negative values for T2D,

443 representing missing information). The above outlier removal steps were repeated for the
444 cardiometabolic traits after excluding the outliers already identified from the cell count data, with the
445 only major modification being the use of logistic regression for the T2D models. This process resulted
446 in the removal of 42 and 53 samples from PCA and null model fitting, respectively.

447 SKAT-O tests of association between *TMBIM1* and the cell count traits identified above were
448 also performed. Similarly to the RVAS in Finnish data, variants within 5kb of *TMBIM1* with MAF < 1%
449 and CADD v1.6 score > 20 were selected for inclusion in this analysis. Rather than the mixed-model
450 version of SKAT-O used in the Finnish data, standard SKAT-O was used due to the lower expected
451 level of cryptic relatedness in the UK Biobank population.

452 We also performed a hypothesis-free, phenome-wide screen of UK Biobank traits to which we
453 had access (**Table S10**), to search for other associations with MT-CN PRS. The statistical models
454 used in this screen were of the same form as those described above, both with and without
455 adjustment for neutrophil and platelet counts. To curate and transform phenotypes, we used an
456 adapted version of PHESANT[61,62]. A few further modifications were made to the pipeline, the most
457 significant being the direct use of logistic regression for testing categorical unordered variables, the
458 inclusion of cancer phenotypes, and the exclusion of sex-specific (or nearly sex-specific) categorical
459 traits. The PHESANT pipeline we used[61] outputs continuous variables both in their raw form and after
460 applying an inverse rank normal transformation. For the sake of being conservative and robust to
461 outliers, we chose to interpret the results from the normalized continuous variables. To control false
462 discovery rate, we performed a Benjamini-Hochberg procedure with Storey correction as
463 implemented in the R package qvalue[63] v2.18.0 on the categorical and normalized continuous
464 variables together. As a secondary analysis, this same correction was applied to the categorical and
465 raw continuous variables together.

466

467 # Results

468 ## Association of MT-CN with metabolic traits

469 We estimated MT-CN in 4,163 individuals from the METSIM and FINRISK studies based on deep
470 (>20x coverage) WGS data. We did so by measuring the mean coverage depth of reads mapped to
471 the mitochondrial genome in each sample, and normalizing it to the mean autosomal coverage (see
472 Material and Methods). We performed batch normalization separately for METSIM and for two
473 FINRISK batches separated by survey years (see Material and Methods). Each measurement was
474 adjusted for age, age^2, and sex, then inverse rank normalized separately before combining across
475 batches. We tested the resulting MT-CN estimates for association with 137 quantitative traits that
476 were collected and normalized according to the procedures described previously[36]. MT-CN was
477 strongly associated with fat mass ($P = 4.48 \times 10^{-16}$) and fasting serum insulin ($P = 2.02 \times 10^{-21}$), as
478 well as numerous additional quantitative traits, many related to metabolic syndrome **(Figure 1a**,
479 **Table S1**). Notably, BMI was significantly associated with MT-CN, although Ding *et al*. did not find
480 evidence of this association[11]. Since population structure was a potential confounder in this analysis
481 considering the presence of mtDNA polymorphisms that might adversely affect short-read alignment,
482 we included SNP-inferred mitochondrial haplogroup as a covariate and reran the tests (**Figure 1b**).
483 The association signals retained significance even after this adjustment.

484 To understand the connection between MT-CN and more clinically relevant phenotypes, we
485 tested our MT-CN estimate against Matsuda ISI and disposition index (**Table 1**), which measure
486 insulin sensitivity and secretion, respectively, and were not included in the initial screen. MT-CN was
487 strongly associated with both insulin phenotypes. Notably, the Matsuda ISI signals survived
488 adjustment for fat mass percentage after excluding diabetic individuals, which indicates that the
489 association of peripheral blood MT-CN with insulin sensitivity was independent of fat mass.

To test for this association signal in a larger cohort, we developed a method to estimate mitochondrial genome copy number using 19,034 samples with whole exome sequencing (WES) data from the METSIM and FINRISK studies that included most of the WGS samples[36] (see Material and Methods). R^2 between WGS-based and WES-based estimates was 0.445 (**Figure S6**). Consistent with the WGS-based analysis, WES-estimated MT-CN was significantly associated with both fat mass and fasting serum insulin levels, even after removing the samples with WGS data, with identical directions of effect (**Table S2**).

Anecdotally, it is interesting to note that these MT association signals can also be detected using read-depth analysis of the nuclear genome (**Figure S1;** manuscript under review[64] - preprint doi: 10.1101/2020.12.13.422502), where reads derived from mtDNA align erroneously to several nuclear loci based on homology between the MT genome and ancient nuclear mitochondrial insertions. This result provides additional evidence for the reported trait associations using an independent MT-CN estimation method, and indicates that these homology-based signals need to be taken into account in future CNV association studies.

Heritability analysis

To assess the extent to which MT-CN is genetically determined, we estimated the heritability of mitochondrial genome copy number using GREML (**Table 2**). We explored two different approaches available: (1) analysis of the 4,149 samples with WGS data that passed quality control measures, where both nuclear genotypes and MT-CN are measured directly from the WGS data, and (2) analysis of the set of 17,718 samples with imputed genotype array data, where MT-CN is estimated from WES data. Of these, (1) benefited from more accurate measurement of genotype and phenotype, whereas (2) had noisier measurements but benefited from larger sample size. We

513 focused primarily on the METSIM cohort, both because of the homogeneity of this cohort (see
514 Material and Methods) and because the number of FINRISK samples with WGS data was small.

515 In the WGS analysis, the GREML-estimated heritability of MT-CN in METSIM was 31% -
516 somewhat less than the 54% value reported in the only prior large-scale study of peripheral blood
517 MT-CN heritability, which was based on low-coverage WGS[11]. For comparison, we used this same
518 approach to estimate heritability of LDL in METSIM WGS data, which yielded an estimate of 34% with
519 a standard error of 7.9% (**Table 3**). This is broadly consistent with prior work[65,66], including analysis of
520 the same Finnish sample set using distinct methods[36] (20.2% heritability). These results show that
521 mitochondrial genome copy number is a genetically determined trait with significant heritability,
522 comparable to that of LDL and other quantitative cardiometabolic traits[36].

523 The analysis of imputed METSIM genotypes using WES-estimated MT-CN yielded an
524 estimated heritability of 11%, which is much lower than the WGS-based estimate (**Table 2**). To
525 understand this discrepancy, we repeated the GREML analysis with the other two combinations of
526 phenotype source (WGS vs. WES estimation) and genotype source (WGS vs. imputed array). When
527 using the WGS-measured phenotype, the estimated heritability decreased only slightly (31% to 27%)
528 when switching from the WGS to imputed genotypes. This suggests that the difference in genotyping
529 method was not the main driver of the observed heritability disparity between the WGS and imputed
530 array datasets. Conversely, when analyzing the imputed METSIM genotypes, switching from
531 WGS-measured to WES-measured MT-CN resulted in a large drop (27% to 11%) in estimated
532 heritability. This suggests that the extra noise inherent in WES-based MT-CN estimates was
533 responsible for the reduction in the GREML-estimated heritability despite the increased sample size
534 of the imputed array dataset.

535

536 **Identification of genetic factors associated with MT-CN**

537 Previous studies have identified three autosomal quantitative trait loci (QTL) reaching genome-wide
538 significance for MT-CN in other populations[25,26]. Another recent study identified two putative QTLs
539 with suggestive P values[27]. We conducted single variant GWAS for MT-CN (see Material and
540 Methods). Analysis of WGS (N = 4,149) and WES (N = 19,034) genotypes yielded no variants
541 exceeding the respective significance thresholds of 5×10^{-8} and 5×10^{-7} (**Figure S2**). However, despite
542 the increased noise in the WES-measured phenotype, GWAS of imputed array genotypes from
543 METSIM (N = 9,791) yielded two loci with genome-wide significant associations, identified by lead
544 markers rs2288464 and rs9389268 (**Figure 2**, **Table 4**). Of the previously-reported MT-CN QTLs[25–27],
545 we observed an inconclusive signal at rs445 (P = 0.048) and a significant signal at rs709591 (P =
546 1.61×10^{-4}), a locus associated with neutrophil count[67,68] (**Table S11**). No significant signal was
547 observed at the other two single-variant QTLs (**Table S11**) or the linkage peak identified by Curran *et*
548 *al*. (**Figure S3**).

549 rs9389268 was the only marker that was strongly associated with MT-CN in the METSIM
550 analyses of both WGS and imputed array data (P = 3.24×10^{-8} and P = 1.26×10^{-10}, respectively).
551 Although this variant was not significantly associated with MT-CN in FINRISK (P = 0.788 and P =
552 0.189 in WGS and imputed array data, respectively) or in a separate random-effects meta-analysis of
553 both cohorts (P = 0.115), the lack of signal in FINRISK is likely the product of lower-quality MT-CN
554 measurements in FINRISK, which displayed heterogeneity across survey years (**Figure S4**). This
555 variant is located in an intergenic region between the *MYB* and *HBS1L* genes, is common across
556 many populations, and is slightly more frequent in Finns compared to non-Finnish Europeans
557 (gnomAD v3 MAF 34.4% vs. 26.0%). *MYB* and *HBS1L* are hematopoietic regulators[69,70], and the
558 region between them is known to be associated with many hematological parameters including fetal
559 hemoglobin levels, hematocrit, and erythrocyte, platelet, and monocyte counts[71–74]. It has been
560 suggested that these intergenic variants function by disrupting *MYB* transcription factor binding and

561 disrupting enhancer-promoter looping[75]. Conditioning the METSIM-only imputed array GWAS on
562 rs9399137 – a tag SNP shown to be associated with many of these hematological parameters[73] –
563 resulted in elimination of the rs9389268 signal entirely (P = 0.408), suggesting that the haplotype
564 responsible for the association of rs9389268 with MT-CN in our data is the same one previously
565 known to be associated with numerous hematological phenotypes.

566 This result is not surprising considering our approach for normalizing MT-CN. Because our
567 MT-CN estimate was based on the ratio of mtDNA coverage to nuclear DNA coverage, changes in
568 the cell type composition of blood could result in changes in our normalized measurement if the
569 underlying cell types have different average numbers of mitochondria. This is especially true of
570 platelets, which can contain mitochondria but not nuclei, and whose counts are known to be
571 associated with rs9399137.

572 rs2288464 seemed to be a good candidate due to its location in the 3' untranslated region of
573 *MRPL34*, which codes for a large subunit protein of the mitochondrial ribosome. While the association
574 signal at this marker was not observed in the WGS data (P = 0.0655), based on the observed effect
575 size of this variant in WES and imputed data as well as the number of WGS datasets available, there
576 was insufficient power (~0.5% at $\alpha = 5\times10^{-7}$) to robustly detect this association in the WGS data[76].

577 We next performed rare variant association (RVAS) analyses using a mixed-model version of
578 SKAT-O[48] to test for genes in which the presence of high-impact rare variants might be associated
579 with MT-CN levels (see Material and Methods; **Figure 3**, **Table 5**). Using WES data, the only gene
580 passing the Bonferroni-adjusted P value threshold of 2.16×10^{-6} was *TMBIM1* (P = 2.96×10^{-8}), a
581 member of a gene family thought to regulate cell death pathways[77]. *TMBIM1* has been shown to be
582 protective against non-alcoholic fatty liver disease (NAFLD), progression to non-alcoholic
583 steatohepatitis, and insulin resistance in mice and macaques[78]. Interestingly, in our analysis - in which
584 a burden test was determined to be optimal by SKAT-O - rare, putatively high-impact variants in

585 *TMBIM1* were associated with a higher MT-CN (**Figure 3c**). Higher MT-CN was, in turn, associated
586 with less severe metabolic syndrome, suggesting that *TMBIM1* is actually a risk gene, not a protective
587 one. Thus, the published function of *TMBIM1* makes it a strong candidate, although the direction of
588 effect in our data disagreed with the direction suggested by prior work in model organisms[78].
589

590 **Inference of causality in the association between MT-CN and insulin**

591 To further understand the association between MT-CN and fasting serum insulin, we employed a
592 Mendelian randomization (MR) approach with MT-CN as the exposure and insulin as the outcome.
593 Using penalized regression, we leveraged our extensive phenotype data to build a genetic instrument
594 from a large number of genetic variants and adjust for possible confounders via a novel approach
595 (see Material and Methods; **Figure 4**). We believe this approach to be more robust to violations of
596 key MR assumptions than other methods in situations where limited data are available and few robust
597 genotype-exposure associations are known. We restricted our analysis to METSIM samples due to
598 batch effects and inconsistencies in available quantitative trait data observed across FINRISK survey
599 years (**Figure S4**). The effect sizes of the instrument in the causality test for insulin levels are shown
600 in **Figure 4d**. We calculated our instrument using either L1 or L2 regularization. In both cases, the
601 MT-CN instrument was not a significant predictor ($\alpha = 0.05$) of insulin when we constructed our
602 instrument from WGS variants, but was significant when the instrument was constructed from
603 imputed array variants. This was likely due to the larger sample size of the imputed array data set.
604 However, the effect estimates were remarkably similar across all four cases. As a result,
605 inverse-variance weighted meta-analysis across datasets yielded highly significant P values for both
606 penalties. In summary, our analysis provided evidence for a significant causal role for MT-CN in
607 determining fasting serum insulin levels that was robust to the choice of regression penalty when

608 building the genetic instrument. We note that this evidence for causality comes with some caveats
609 (see Material and Methods).
610

611 **Replication and biological interpretation**

612 In principle, changes in MT-CN can be caused by changes in the number of mitochondrial genome
613 copies within cells or by changes in the blood cell type composition. Based on the association with
614 rs9389268 and the nuances of the normalization procedure described above, we sought to test the
615 hypothesis that our MT-CN measurement primarily reflects the cell type composition of the blood
616 rather than the number of mitochondria per cell. We used imputed array genotype and phenotype
617 data from the UK Biobank (N = 357,656) for this purpose[79].

618 We first tested cell counts from the UK Biobank (UKBB) against a polygenic risk score (PRS)
619 for MT-CN built using the genetic instrument from the Finnish data. Leukocyte, neutrophil, and platelet
620 counts were all significantly associated with MT-CN PRS conditional on age, age^2, and sex (see
621 Material and Methods, **Table 6**). However, adjusting for neutrophil counts in the leukocyte regression
622 eliminated the signal (PRS regression coefficient P = 0.839), suggesting that the leukocyte count
623 signal was driven by the effect of neutrophil count. We removed any high leverage, large residual
624 samples and repeated the neutrophil and platelet count regressions to ensure that this result was
625 robust to outliers and found no appreciable change in significance (**Table 6**). As a result, we
626 concluded that our MT-CN measurement was significantly associated with neutrophil and platelet
627 counts. Subsequent analyses were performed both with and without adjustment for these variables,
628 as described below.

629 We note that the effect directions of the associations of platelet counts with metS and MT-CN
630 PRS seem inconsistent at first glance, as platelet counts were positively correlated with MT-CN PRS
631 (**Table 6**) and metS (**Table S3**) while MT-CN and insulin (a proxy for metS) were negatively correlated

632 (**Figure 1b**). However, the FinMetSeq regression model in **Figure 1b** was not conditional on any
633 other covariates (although age, age^2, and sex were regressed out of the MT-CN measurement prior to
634 this analysis), while the UKBB models that gave rise to **Table 6** and **Table S3** adjusted for many
635 additional covariates, including 20 PCs and age-sex interaction terms. As a result, the effect
636 directions for the analyses in the two datasets are not directly comparable.

637 We next tested for associations between MT-CN PRS and several cardiometabolic phenotypes
638 from the test in **Figure 1a** (see Material and Methods). With the exception of C-reactive protein, which
639 showed no significant association, all tested phenotypes showed nominal association with MT-CN
640 PRS at $\alpha = 0.05$, with total triglycerides and HDL being the only traits surviving Bonferroni correction
641 (**Table 7**). We interpret this as replication of the link between mitochondrial genome copy number and
642 metabolic syndrome in a large, independent data set.

643 To determine whether there was any association between MT-CN and metabolic syndrome not
644 mediated through cell counts, we repeated the tests of cardiometabolic trait association with MT-CN
645 PRS with adjustment for platelet and neutrophil counts. HDL was the only trait with a nominal ($\alpha =$
646 0.05) association with PRS under this adjustment, but this signal was not strong enough to survive
647 Bonferroni correction (**Table 7**). This suggests that the associations we observed between MT-CN
648 and metabolic traits arose simply because MT-CN is a proxy for platelet and neutrophil count. This
649 was supported by the fact that direct testing of platelets and neutrophils against triglycerides, fat
650 mass, and HDL yielded remarkably significant associations, which survived *post-hoc* removal of
651 high-leverage, high-residual outlier samples (**Table S3**). This evidence for MT-CN as a proxy for
652 platelet and neutrophil counts strongly suggests that the causal relationship observed in the
653 Mendelian randomization experiment (see above) in fact represents a causative role for neutrophils
654 and platelet counts in setting serum insulin levels.

655 Given the strong observed associations between blood cell count phenotypes and MT-CN
656 PRS, we used these blood phenotypes to seek replication of the genetic associations detected in
657 Finnish data. Using imputed UKBB genotype data, we tested the expected alternate allele dosage of
658 both rs2288464 and rs9389268 against the same blood cell traits mentioned above, using linear
659 regression (**Table S4**; expected alternate allele dosage was calculated from genotype call
660 probabilities as $DS = P(0/1) + 2P(1/1)$). As expected given its known associations with multiple
661 hematological parameters (see above), rs9389268 showed strong associations with all tested blood
662 cell phenotypes. rs2288464 was not significantly associated with any of the five phenotypes after
663 correction for multiple testing, although a nominal association was detected with total leukocyte count.
664 This further strengthens our belief that rs9389268 is truly associated with MT-CN through blood cell
665 composition. We also tested *TMBIM1* against the same blood cell traits in UKBB using SKAT-O[48], and
666 found no significant associations (**Table S4**). This may mean that *TMBIM1* affects MT-CN through a
667 mechanism other than altering blood cell type composition.

668 As further evidence that MT-CN is a proxy for blood cell composition, we looked up MT-CN
669 association P values in METSIM for the top five neutrophil and platelet count QTLs from the
670 NHGRI-EBI GWAS Catalog. Out of ten variants tested, five had $P < 0.05$ in METSIM (**Table S11**). We
671 note that three of these five were either near or identical to known MT-CN loci (including rs9389268,
672 the marker identified in this study). rs25645, a variant reported to be highly associated with neutrophil
673 count[68], is only 2.5 kb away from rs709591, a SNP with a reported suggestive association with
674 MT-CN[27] and a P value of 1.61×10^{-4} in our METSIM study. Moreover, rs11759553, a
675 platelet-associated variant[68], is 324 kb away from rs9389268, the lead marker for MT-CN in METSIM
676 (rs11759553 $P = 2.15\times10^{-10}$ in METSIM). Finally, rs445 was reported as a lead marker for both
677 MT-CN association[25] and platelet count[68]. rs445 has $P = 0.048$ for association with MT-CN in
678 METSIM. While none of the 10 known cell count-associated markers tested achieved significance

679 beyond a Bonferroni threshold, the overlap between these variants and independently-measured
680 MT-CN QTLs was suggestive of a relationship between cell counts and whole blood-derived MT-CN.

681 Using UKBB data, we further sought to generate hypotheses for other phenotypic associations
682 with MT-CN. To this end, we performed a phenome-wide screen of MT-CN PRS against all of the
683 UKBB phenotypes available to us. To curate and transform these phenotypes, we used a modified
684 version of PHESANT[61,62], which outputs all continuous variables in both raw and inverse
685 rank-normalized form. We chose to interpret the results from the normalized continuous variables
686 (**Table S5**) to be conservative and robust to outliers, although the results of the raw continuous
687 variable analyses were similar (**Table S6**). No metabolic syndrome traits appeared among the tested
688 traits with $q < 0.05$. However, the tests for HDL cholesterol, self-reported heart attack, and
689 doctor-diagnosed heart attack did yield somewhat suggestive results ($q = 0.123$, 0.176, and 0.176,
690 respectively). We also repeated this screen with adjustment for neutrophil and platelet counts (**Table**
691 **S7** and **Table S8**), resulting again in no metabolic syndrome phenotypes achieving $q < 0.05$. The
692 addition of neutrophil and platelet counts as covariates attenuated the suggestive signals for HDL
693 cholesterol, self-reported heart attack, and doctor-diagnosed heart attack ($q = 0.284$, 0.391, and
694 0.402, respectively).

695

696 ## Discussion

697 We have described one of the most well-powered studies to date of the genetic relationship
698 between MT-CN measurements in blood and cardiometabolic phenotypes. Our study is one of very
699 few of which we are aware to utilize WGS data, found to be the most reliable method for estimating
700 MT-CN in a recent study[18], for this purpose. Our data show highly significant associations between
701 blood-derived MT-CN measurements and several cardiometabolic traits, particularly insulin and fat
702 mass. We observed strong heritability of MT-CN (31%), on par with other widely studied

703 cardiometabolic traits such as LDL, and identified one single marker association on a haplotype
704 previously associated with several hematological parameters[71–74]. A previous study using qPCR to
705 quantify MT-CN reported two sub-threshold QTLs[27]; of these markers, only rs709591 replicated in our
706 study ($P = 1.61\times10^{-4}$). We also report one gene with a rare-variant association with MT-CN, *TMBIM1*,
707 that has a known link to non-alcoholic fatty liver disease[78]. More work is needed to replicate this
708 genetic association.

709 Using a novel multiple-variant instrument-building method, we report evidence from Mendelian
710 randomization supporting a causal role for MT-CN in metabolic syndrome. Further, we used UK
711 Biobank data to show that not only does the link between MT-CN and metabolic syndrome replicate in
712 an independent data set using a polygenic risk score approach. Contrary to previous claims that
713 variability in the number of mitochondria per cell is responsible for CHD risk[12], this association is
714 mediated by neutrophil and platelet counts.

715 One important question that our study cannot definitively resolve is the relative contribution of
716 intracellular mitochondrial abundance versus cell-type composition differences in determining the
717 measured MT-CN value. We identified a MT-CN association result at a known QTL for cell type
718 composition of blood[71–74] (HBS1L-MYB), and we further replicated a prior sub-threshold association at
719 a different neutrophil-associated locus[67,68] (rs709591). Together, these results argue that cell type
720 composition is an important component of this measurement. On the other hand, two other significant
721 associations from the Finnish dataset (rs2288464, *TMBIM1*) showed no effect on cell type
722 composition in the UK Biobank. Future work in large cohorts with both WGS and cell count data –
723 which were not simultaneously measured in any samples in this study – will be required to rigorously
724 determine what blood-derived MT-CN primarily measures. However, the results of our MR and UK
725 Biobank analyses together suggest that MT-CN is causally related to metabolic syndrome traits, and
726 that this relationship is mediated by cell-type composition differences.

There is prior evidence to support the role of inflammation – specifically via innate immune cells such as neutrophils – in the etiology of type 2 diabetes (T2D) and insulin resistance[80–82], which suggests a plausible model by which peripheral blood neutrophil count could influence metabolic syndrome. Nutrient excess and high fat diets are known to recruit neutrophils into tissues, which then cause insulin resistance both by releasing TNF-α and IL-6 and by upregulating cyclooxygenase[80]. This leads to increased LTB4 and subsequent upregulation of NF-κB, a central regulator of inflammation. Moreover, free fatty acids also cause neutrophils to stay in tissues longer, resulting in persistent inflammation and leading to insulin resistance[80]. While it is known that inflammation, and particularly neutrophils, play a role in metabolic syndrome, our results strongly suggest that peripheral blood neutrophil count causally contributes to this process and is associated with heritable genetic variation in the human population. Overall, our work provides further insight into the role that inflammation plays in metabolic syndrome and supports the idea that targeting inflammation may be a fruitful avenue of investigation in developing future therapeutics.

Supplemental Information Description

Supplemental data include 8 figures and 11 tables.

Acknowledgements

This work was funded by the NHGRI Centers for Common Disease Genetics (grant number UM1 HG008853 to I.M.H. and N.O.S), the NHGRI large-scale sequencing grant (grant number 5U54HG003079), the Sigrid Jusélius Foundation (to S.R.), the University of Helsinki HiLIFE Fellow grants 2017-2020 (to S.R.), the Academy of Finland Center of Excellence in Complex Disease Genetics (grant number 312062 to S.R.), the Academy of Finland (grant number 285380 to S.R.), the

750 National Heart, Lung and Blood Institute (grant number T32HL007081 to E.Y.), and the National
751 Center for Advancing Translational Sciences (grant number UL1TR002345 to E.Y.).
752 We thank Hyeim Jung for her help in identifying outlier individuals as well as the WashU data
753 production team, in particular Robert Fulton, Lucinda Fulton, Catrina Fronick, Aye Wollam and Susan
754 K. Dutcher. This research has been conducted using the UK Biobank Resource under Application
755 Number 56546. The FINRISK samples used for the research were obtained from the FINRISK Study
756 and from THL Biobank. We thank all study participants for their generous participation at THL
757 Biobank and the FINRISK Study.
758

759 ## Declaration of Interests

760 N.O.S has received grant funding from Regeneron Pharmaceuticals for unrelated work. The rest of
761 the authors declare no competing interests.
762

763 ## Web Resources

764 EPACTS, https://genome.sph.umich.edu/wiki/EPACTS
765 lmPerm, https://github.com/mtorchiano/lmPerm
766 NHGRI-EBI GWAS Catalog, https://www.ebi.ac.uk/gwas
767 smartPCA, https://github.com/DReichLab/EIG
768

769 ## Data and Code Availability

770 METSIM WGS, METSIM WES, and FINRISK WES sequence data are available through dbGaP
771 (accession numbers phs001579, phs000752, and phs000756). METSIM callsets from WGS and
772 imputed array data as well as MT-CN phenotype values will soon be available through AnVIL.

773 Imputed array GWAS summary statistics from METSIM and and WES SKAT-O summary statistics
774 from the joint dataset are freely available at
775 https://wustl.box.com/s/7xfbmxq2r4kg8p8bfc7vpqlrmqvhm0lx. Genomic and phenotypic data for the
776 FINRISK cohort are obtainable through THL Biobank, the Finnish Institute for Health and Welfare,
777 Finland (https://thl.fi/en/web/thl-biobank).

778

779 **References**

780 1. Koliaki, C., and Roden, M. (2016). Alterations of Mitochondrial Function and Insulin Sensitivity in Human
781 Obesity and Diabetes Mellitus | Annual Review of Nutrition. Annu. Rev. Nutr. *36*, 337–367.

782 2. Weisberg, S.P., McCann, D., Desai, M., Rosenbaum, M., Leibel, R.L., and Ferrante, A.W. (2003). Obesity is
783 associated with macrophage accumulation in adipose tissue. J. Clin. Invest. *112*, 1796–1808.

784 3. Kim, J.-A., Wei, Y., and Sowers, J.R. (2008). Role of Mitochondrial Dysfunction in Insulin Resistance. Circ.
785 Res. *102*, 401–414.

786 4. Burgueño, A.L., Cabrerizo, R., Gonzales Mansilla, N., Sookoian, S., and Pirola, C.J. (2013). Maternal
787 high-fat intake during pregnancy programs metabolic-syndrome-related phenotypes through liver mitochondrial
788 DNA copy number and transcriptional activity of liver PPARGC1A. J. Nutr. Biochem. *24*, 6–13.

789 5. Sookoian, S., Rosselli, M.S., Gemma, C., Burgueño, A.L., Gianotti, T.F., Castaño, G.O., and Pirola, C.J.
790 (2010). Epigenetic regulation of insulin resistance in nonalcoholic fatty liver disease: Impact of liver methylation
791 of the peroxisome proliferator–activated receptor γ coactivator 1α promoter. Hepatology *52*, 1992–2000.

792 6. Begriche, K., Igoudjil, A., Pessayre, D., and Fromenty, B. (2006). Mitochondrial dysfunction in NASH:
793 Causes, consequences and possible means to prevent it. Mitochondrion *6*, 1–28.

794 7. Zhou, X., Li, R., Liu, X., Wang, L., Hui, P., Chan, L., Saha, P.K., and Hu, Z. (2016). ROCK1 reduces
795 mitochondrial content and irisin production in muscle suppressing adipocyte browning and impairing insulin
796 sensitivity. Sci. Rep. *6*, 29669.

797 8. Ren, J., Pulakat, L., Whaley-Connell, A., and Sowers, J.R. (2010). Mitochondrial biogenesis in the metabolic
798 syndrome and cardiovascular disease. J. Mol. Med. *88*, 993–1001.

799 9. Stephenson, E.J., and Hawley, J.A. (2014). Mitochondrial function in metabolic health: A genetic and
800 environmental tug of war. Biochimica et Biophysica Acta (BBA) - General Subjects *1840*, 1285–1294.

801 10. Szendroedi, J., Phielix, E., and Roden, M. (2012). The role of mitochondria in insulin resistance and type 2
802 diabetes mellitus. Nat. Rev. Endocrinol. *8*, 92–103.

803 11. Ding, J., Sidore, C., Butler, T.J., Wing, M.K., Qian, Y., Meirelles, O., Busonero, F., Tsoi, L.C., Maschio, A.,
804 Angius, A., et al. (2015). Assessing Mitochondrial DNA Variation and Copy Number in Lymphocytes of ~2,000
805 Sardinians Using Tailored Sequencing Analysis Tools. PLoS Genet. *11*, e1005306.

806 12. Chen, S., Xie, X., Wang, Y., Gao, Y., Xie, X., Yang, J., and Ye, J. (2014). Association between leukocyte
807 mitochondrial DNA content and risk of coronary heart disease: A case-control study. Atherosclerosis *237*,
808 220–226.

809 13. Lee, H.K., Song, J.H., Shin, C.S., Park, D.J., Park, K.S., Lee, K.U., and Koh, C.-S. (1998). Decreased
810 mitochondrial DNA content in peripheral blood precedes the development of non-insulin-dependent diabetes
811 mellitus. Diabetes Res. Clin. Pract. *42*, 161–167.

812 14. Shoar, Z., Goldenthal, M.J., De Luca, F., and Suarez, E. (2016). Mitochondrial DNA content and function,
813 childhood obesity, and insulin resistance. Endocr. Res. *41*, 49–56.

814 15. Song, J., Oh, J.Y., Sung, Y.-A., Pak, Y.K., Park, K.S., and Lee, H.K. (2001). Peripheral Blood Mitochondrial
815 DNA Content Is Related to Insulin Sensitivity in Offspring of Type 2 Diabetic Patients. Diabetes Care *24*,
816 865–869.

817 16. Weng, S.-W., Lin, T.-K., Liou, C.-W., Chen, S.-D., Wei, Y.-H., Lee, H.-C., Chen, I.-Y., Hsieh, C.-J., and
818 Wang, P.-W. (2009). Peripheral blood mitochondrial DNA content and dysregulation of glucose metabolism.
819 Diabetes Res. Clin. Pract. *83*, 94–99.

820 17. Liu, L.-P., Cheng, K., Ning, M.-A., Li, H.-H., Wang, H.-C., Li, F., Chen, S.-Y., Qu, F.-L., and Guo, W.-Y.
821 (2017). Association between peripheral blood cells mitochondrial DNA content and severity of coronary heart
822 disease. Atherosclerosis *261*, 105–110.

823 18. Longchamps, R.J., Castellani, C.A., Yang, S.Y., Newcomb, C.E., Sumpter, J.A., Lane, J., Grove, M.L.,
824 Guallar, E., Pankratz, N., Taylor, K.D., et al. (2020). Evaluation of mitochondrial DNA copy number estimation
825 techniques. PLoS One *15*, e0228166.

826 19. Guyatt, A.L., Burrows, K., Guthrie, P.A.I., Ring, S., McArdle, W., Day, I.N.M., Ascione, R., Lawlor, D.A.,
827 Gaunt, T.R., and Rodriguez, S. (2018). Cardiometabolic phenotypes and mitochondrial DNA copy number in
828 two cohorts of UK women. Mitochondrion *39*, 9–19.

829 20. Ashar, F.N., Zhang, Y., Longchamps, R.J., Lane, J., Moes, A., Grove, M.L., Mychaleckyj, J.C., Taylor, K.D.,
830 Coresh, J., Rotter, J.I., et al. (2017). Association of Mitochondrial DNA Copy Number With Cardiovascular
831 Disease. JAMA Cardiol *2*, 1247–1255.

832 21. Robin, E.D., and Wong, R. (1988). Mitochondrial DNA molecules and virtual number of mitochondria per
833 cell in mammalian cells. J. Cell. Physiol. *136*, 507–513.

834 22. Maianski, N.A., Geissler, J., Srinivasula, S.M., Alnemri, E.S., Roos, D., and Kuijpers, T.W. (2004).
835 Functional characterization of mitochondria in neutrophils: a role restricted to apoptosis. Cell Death Differ. *11*,
836 143–153.

837 23. Zharikov, S., and Shiva, S. (2013). Platelet mitochondrial function: from regulation of thrombosis to
838 biomarker of disease. Biochem. Soc. Trans. *41*, 118–123.

839 24. Cai, N., Chang, S., Li, Y., Li, Q., Hu, J., Liang, J., Song, L., Kretzschmar, W., Gan, X., Nicod, J., et al.
840 (2015). Molecular signatures of major depression. Curr. Biol. *25*, 1146–1156.

841 25. Cai, N., Li, Y., Chang, S., Liang, J., Lin, C., Zhang, X., Liang, L., Hu, J., Chan, W., Kendler, K.S., et al.
842 (2015). Genetic Control over mtDNA and Its Relationship to Major Depressive Disorder. Curr. Biol. *25*,
843 3170–3177.

844 26. Curran, J.E., Johnson, M.P., Dyer, T.D., Göring, H.H.H., Kent, J.W., Charlesworth, J.C., Borg, A.J., Jowett,
845 J.B.M., Cole, S.A., MacCluer, J.W., et al. (2007). Genetic determinants of mitochondrial content. Hum. Mol.

Genet. *16*, 1504–1514.

27. Guyatt, A.L., Brennan, R.R., Burrows, K., Guthrie, P.A.I., Ascione, R., Ring, S.M., Gaunt, T.R., Pyle, A., Cordell, H.J., Lawlor, D.A., et al. (2019). A genome-wide association study of mitochondrial DNA copy number in two population-based cohorts. Hum. Genomics *13*, 6.

28. Pajukanta, P., Terwilliger, J.D., Perola, M., Hiekkalinna, T., Nuotio, I., Ellonen, P., Parkkonen, M., Hartiala, J., Ylitalo, K., Pihlajamäki, J., et al. (1999). Genomewide scan for familial combined hyperlipidemia genes in finnish families, suggesting multiple susceptibility loci influencing triglyceride, cholesterol, and apolipoprotein B levels. Am. J. Hum. Genet. *64*, 1453–1463.

29. Pajukanta, P., Allayee, H., Krass, K.L., Kuraishy, A., Soro, A., Lilja, H.E., Mar, R., Taskinen, M.-R., Nuotio, I., Laakso, M., et al. (2003). Combined analysis of genome scans of dutch and finnish families reveals a susceptibility locus for high-density lipoprotein cholesterol on chromosome 16q. Am. J. Hum. Genet. *72*, 903–917.

30. Laakso, M., Kuusisto, J., Stančáková, A., Kuulasmaa, T., Pajukanta, P., Lusis, A.J., Collins, F.S., Mohlke, K.L., and Boehnke, M. (2017). The Metabolic Syndrome in Men study: a resource for studies of metabolic and cardiovascular diseases. J. Lipid Res. *58*, 481–493.

31. Borodulin, K., Tolonen, H., Jousilahti, P., Jula, A., Juolevi, A., Koskinen, S., Kuulasmaa, K., Laatikainen, T., Männistö, S., Peltonen, M., et al. (2018). Cohort Profile: The National FINRISK Study. Int. J. Epidemiol. *47*, 696–696i.

32. (2019). Picard Toolkit (Broad Institute, GitHub repository).

33. Li, H., Handsaker, B., Wysoker, A., Fennell, T., Ruan, J., Homer, N., Marth, G., Abecasis, G., Durbin, R., and 1000 Genome Project Data Processing Subgroup (2009). The Sequence Alignment/Map format and SAMtools. Bioinformatics *25*, 2078–2079.

34. Jun, G., Flickinger, M., Hetrick, K.N., Romm, J.M., Doheny, K.F., Abecasis, G.R., Boehnke, M., and Kang, H.M. (2012). Detecting and estimating contamination of human DNA samples in sequencing and array-based genotype data. Am. J. Hum. Genet. *91*, 839–848.

35. McCarthy, S., Das, S., Kretzschmar, W., Delaneau, O., Wood, A.R., Teumer, A., Kang, H.M., Fuchsberger, C., Danecek, P., Sharp, K., et al. (2016). A reference panel of 64,976 haplotypes for genotype imputation. Nat. Genet. *48*, 1279–1283.

36. Locke, A.E., Steinberg, K.M., Chiang, C.W.K., Service, S.K., Havulinna, A.S., Stell, L., Pirinen, M., Abel, H.J., Chiang, C.C., Fulton, R.S., et al. (2019). Exome sequencing of Finnish isolates enhances rare-variant association power. Nature *572*, 323–328.

37. DePristo, M.A., Banks, E., Poplin, R., Garimella, K.V., Maguire, J.R., Hartl, C., Philippakis, A.A., del Angel, G., Rivas, M.A., Hanna, M., et al. (2011). A framework for variation discovery and genotyping using next-generation DNA sequencing data. Nat. Genet. *43*, 491–498.

38. Tan, A., Abecasis, G.R., and Kang, H.M. (2015). Unified representation of genetic variants. Bioinformatics *31*, 2202–2204.

39. Manichaikul, A., Mychaleckyj, J.C., Rich, S.S., Daly, K., Sale, M., and Chen, W.-M. (2010). Robust relationship inference in genome-wide association studies. Bioinformatics *26*, 2867–2873.

40. Quinlan, A.R., and Hall, I.M. (2010). BEDTools: a flexible suite of utilities for comparing genomic features.

885 Bioinformatics *26*, 841–842.

886 41. Fromer, M., Moran, J.L., Chambert, K., Banks, E., Bergen, S.E., Ruderfer, D.M., Handsaker, R.E.,
887 McCarroll, S.A., O'Donovan, M.C., Owen, M.J., et al. (2012). Discovery and statistical genotyping of
888 copy-number variation from whole-exome sequencing depth. Am. J. Hum. Genet. *91*, 597–607.

889 42. Kloss-Brandstätter, A., Pacher, D., Schönherr, S., Weissensteiner, H., Binna, R., Specht, G., and
890 Kronenberg, F. (2011). HaploGrep: a fast and reliable algorithm for automatic classification of mitochondrial
891 DNA haplogroups. Hum. Mutat. *32*, 25–32.

892 43. Yang, J., Lee, S.H., Goddard, M.E., and Visscher, P.M. (2011). GCTA: a tool for genome-wide complex trait
893 analysis. Am. J. Hum. Genet. *88*, 76–82.

894 44. Lee, S.H., Wray, N.R., Goddard, M.E., and Visscher, P.M. (2011). Estimating missing heritability for disease
895 from genome-wide association studies. Am. J. Hum. Genet. *88*, 294–305.

896 45. Yang, J., Bakshi, A., Zhu, Z., Hemani, G., Vinkhuyzen, A.A.E., Lee, S.H., Robinson, M.R., Perry, J.R.B.,
897 Nolte, I.M., van Vliet-Ostaptchouk, J.V., et al. (2015). Genetic variance estimation with imputed variants finds
898 negligible missing heritability for human height and body mass index. Nat. Genet. *47*, 1114–1120.

899 46. Evans, L.M., Tahmasbi, R., Vrieze, S.I., Abecasis, G.R., Das, S., Gazal, S., Bjelland, D.W., de Candia, T.R.,
900 Haplotype Reference Consortium, Goddard, M.E., et al. (2018). Comparison of methods that use whole
901 genome data to estimate the heritability and genetic architecture of complex traits. Nat. Genet. *50*, 737–745.

902 47. Balduzzi, S., Rücker, G., and Schwarzer, G. (2019). How to perform a meta-analysis with R: a practical
903 tutorial. Evid. Based. Ment. Health *22*, 153–160.

904 48. Lee, S., Emond, M.J., Bamshad, M.J., Barnes, K.C., Rieder, M.J., Nickerson, D.A., NHLBI GO Exome
905 Sequencing Project—ESP Lung Project Team, Christiani, D.C., Wurfel, M.M., and Lin, X. (2012). Optimal
906 unified approach for rare-variant association testing with application to small-sample case-control whole-exome
907 sequencing studies. Am. J. Hum. Genet. *91*, 224–237.

908 49. Kircher, M., Witten, D.M., Jain, P., O'Roak, B.J., Cooper, G.M., and Shendure, J. (2014). A general
909 framework for estimating the relative pathogenicity of human genetic variants. Nat. Genet. *46*, 310–315.

910 50. McLaren, W., Gil, L., Hunt, S.E., Riat, H.S., Ritchie, G.R.S., Thormann, A., Flicek, P., and Cunningham, F.
911 (2016). The Ensembl Variant Effect Predictor. Genome Biol. *17*, 122.

912 51. Palmer, T.M., Lawlor, D.A., Harbord, R.M., Sheehan, N.A., Tobias, J.H., Timpson, N.J., Davey Smith, G.,
913 and Sterne, J.A.C. (2012). Using multiple genetic variants as instrumental variables for modifiable risk factors.
914 Stat. Methods Med. Res. *21*, 223–242.

915 52. Friedman, J., Hastie, T., and Tibshirani, R. (2010). Regularization Paths for Generalized Linear Models via
916 Coordinate Descent. J. Stat. Softw. *33*, 1–22.

917 53. Chang, C.C., Chow, C.C., Tellier, L.C., Vattikuti, S., Purcell, S.M., and Lee, J.J. (2015). Second-generation
918 PLINK: rising to the challenge of larger and richer datasets. Gigascience *4*, 7.

919 54. Burgess, S., and Thompson, S.G. (2013). Use of allele scores as instrumental variables for Mendelian
920 randomization. Int. J. Epidemiol. *42*, 1134–1144.

921 55. Beasley, T.M., Erickson, S., and Allison, D.B. (2009). Rank-based inverse normal transformations are
922 increasingly used, but are they merited? Behav. Genet. *39*, 580–595.

56. Blom, G. (1958). Statistical estimates and transformed beta-variables. Almqvist & Wiksell.

57. van Buuren, S., and Groothuis-Oudshoorn, K. (2011). mice: Multivariate Imputation by Chained Equations in R. Journal of Statistical Software, Articles *45*, 1–67.

58. Honaker, J., King, G., and Blackwell, M. (2011). Amelia II: A Program for Missing Data. Journal of Statistical Software, Articles *45*, 1–47.

59. Cole, S.R., Platt, R.W., Schisterman, E.F., Chu, H., Westreich, D., Richardson, D., and Poole, C. (2010). Illustrating bias due to conditioning on a collider. Int. J. Epidemiol. *39*, 417–420.

60. VanderWeele, T.J., Tchetgen Tchetgen, E.J., Cornelis, M., and Kraft, P. (2014). Methodological challenges in mendelian randomization. Epidemiology *25*, 427–435.

61. Neale, B. Neale Lab UK Biobank Analysis.

62. Millard, L.A.C., Davies, N.M., Gaunt, T.R., Davey Smith, G., and Tilling, K. (2018). Software Application Profile: PHESANT: a tool for performing automated phenome scans in UK Biobank. Int. J. Epidemiol. *47*, 29–35.

63. Storey, J.D., Bass, A.J., Dabney, A., and Robinson, D. (2019). qvalue: Q-value estimation for false discovery rate control.

64. Chen, L., Abel, H.J., Das, I., Larson, D.E., Ganel, L., Kanchi, K.L., Regier, A.A., Young, E.P., Kang, C.J., Scott, A.J., et al. (2020). Association of Structural Variation with Cardiometabolic Traits in Finns.

65. Kaess, B., Fischer, M., Baessler, A., Stark, K., Huber, F., Kremer, W., Kalbitzer, H.R., Schunkert, H., Riegger, G., and Hengstenberg, C. (2008). The lipoprotein subfraction profile: heritability and identification of quantitative trait loci. J. Lipid Res. *49*, 715–723.

66. Weiss, L.A., Pan, L., Abney, M., and Ober, C. (2006). The sex-specific genetic architecture of quantitative traits in humans. Nat. Genet. *38*, 218–222.

67. Nalls, M.A., Couper, D.J., Tanaka, T., van Rooij, F.J.A., Chen, M.-H., Smith, A.V., Toniolo, D., Zakai, N.A., Yang, Q., Greinacher, A., et al. (2011). Multiple loci are associated with white blood cell phenotypes. PLoS Genet. *7*, e1002113.

68. Chen, M.-H., Raffield, L.M., Mousas, A., Sakaue, S., Huffman, J.E., Moscati, A., Trivedi, B., Jiang, T., Akbari, P., Vuckovic, D., et al. (2020). Trans-ethnic and Ancestry-Specific Blood-Cell Genetics in 746,667 Individuals from 5 Global Populations. Cell *182*, 1198–1213.e14.

69. Wang, X., Angelis, N., and Thein, S.L. (2018). MYB - A regulatory factor in hematopoiesis. Gene *665*, 6–17.

70. Pandit, R.A., Svasti, S., Sripichai, O., Munkongdee, T., Triwitayakorn, K., Winichagoon, P., Fucharoen, S., and Peerapittayamongkol, C. (2008). Association of SNP in exon 1 of HBS1L with hemoglobin F level in beta0-thalassemia/hemoglobin E. Int. J. Hematol. *88*, 357–361.

71. Thein, S.L., Menzel, S., Peng, X., Best, S., Jiang, J., Close, J., Silver, N., Gerovasilli, A., Ping, C., Yamaguchi, M., et al. (2007). Intergenic variants of HBS1L-MYB are responsible for a major quantitative trait locus on chromosome 6q23 influencing fetal hemoglobin levels in adults. Proceedings of the National Academy of Sciences *104*, 11346–11351.

72. Ganesh, S.K., Zakai, N.A., van Rooij, F.J.A., Soranzo, N., Smith, A.V., Nalls, M.A., Chen, M.-H., Kottgen,

961 A., Glazer, N.L., Dehghan, A., et al. (2009). Multiple loci influence erythrocyte phenotypes in the CHARGE
962 Consortium. Nat. Genet. *41*, 1191–1198.

963 73. Menzel, S., Jiang, J., Silver, N., Gallagher, J., Cunningham, J., Surdulescu, G., Lathrop, M., Farrall, M.,
964 Spector, T.D., and Thein, S.L. (2007). The HBS1L-MYB intergenic region on chromosome 6q23.3 influences
965 erythrocyte, platelet, and monocyte counts in humans. Blood *110*, 3624–3626.

966 74. Lin, B.D., Carnero-Montoro, E., Bell, J.T., Boomsma, D.I., de Geus, E.J., Jansen, R., Kluft, C., Mangino, M.,
967 Penninx, B., Spector, T.D., et al. (2017). 2SNP heritability and effects of genetic variants for
968 neutrophil-to-lymphocyte and platelet-to-lymphocyte ratio. J. Hum. Genet. *62*, 979–988.

969 75. Stadhouders, R., Aktuna, S., Thongjuea, S., Aghajanirefah, A., Pourfarzad, F., van Ijcken, W., Lenhard, B.,
970 Rooks, H., Best, S., Menzel, S., et al. (2014). HBS1L-MYB intergenic variants modulate fetal hemoglobin via
971 long-range MYB enhancers. J. Clin. Invest. *124*, 1699–1710.

972 76. Purcell, S., Cherny, S.S., and Sham, P.C. (2003). Genetic Power Calculator: design of linkage and
973 association genetic mapping studies of complex traits. Bioinformatics *19*, 149–150.

974 77. Zhou, J., Zhu, T., Hu, C., Li, H., Chen, G., Xu, G., Wang, S., Zhou, J., and Ma, D. (2008). Comparative
975 genomics and function analysis on BI1 family. Comput. Biol. Chem. *32*, 159–162.

976 78. Zhao, G.-N., Zhang, P., Gong, J., Zhang, X.-J., Wang, P.-X., Yin, M., Jiang, Z., Shen, L.-J., Ji, Y.-X., Tong,
977 J., et al. (2017). Tmbim1 is a multivesicular body regulator that protects against non-alcoholic fatty liver
978 disease in mice and monkeys by targeting the lysosomal degradation of Tlr4. Nat. Med. *23*, 742–752.

979 79. Sudlow, C., Gallacher, J., Allen, N., Beral, V., Burton, P., Danesh, J., Downey, P., Elliott, P., Green, J.,
980 Landray, M., et al. (2015). UK biobank: an open access resource for identifying the causes of a wide range of
981 complex diseases of middle and old age. PLoS Med. *12*, e1001779.

982 80. Welty, F.K., Alfaddagh, A., and Elajami, T.K. (2016). Targeting inflammation in metabolic syndrome. Transl.
983 Res. *167*, 257–280.

984 81. Creely, S.J., McTernan, P.G., Kusminski, C.M., Fisher, ff M., Da Silva, N.F., Khanolkar, M., Evans, M.,
985 Harte, A.L., and Kumar, S. (2007). Lipopolysaccharide activates an innate immune system response in human
986 adipose tissue in obesity and type 2 diabetes. Am. J. Physiol. Endocrinol. Metab. *292*, E740–E747.

987 82. Hotamisligil, G.S. (2017). Inflammation, metaflammation and immunometabolic disorders. Nature *542*,
988 177–185.

989

990 Figure Titles and Legends

991 **Figure 1. Cardiometabolic trait associations with MT-CN in WGS data.** (A) Phenome-wide
992 association study of normalized MT-CN against 137 cardiometabolic traits in the 4,163 sample data
993 set. Traits are grouped into 17 categories, represented by the color of each bar. The top three most
994 significant traits are, in order: fasting serum insulin, C-reactive protein, and fat mass. Exact P values

995 and effect estimates, as calculated by EMMAX, are listed in **Table S1**. (B) Association tests between
996 normalized MT-CN and both fat mass and fasting serum insulin using WGS data (N = 4,163). Results
997 are shown for the EMMAX test and a permutation test in which mitochondrial haplogroups were
998 adjusted for.

999

1000 **Figure 2. Single-marker genetic associations with MT-CN in imputed array data.** (A) Manhattan
1001 plot for a genome-wide association test of normalized, WES-measured MT-CN using imputed array
1002 genotype data from METSIM (N = 9,791). Two loci markers reached the genome-wide significance of
1003 5×10^{-8}, identified by lead markers rs2288464 and rs9389268. (B) Quantile-quantile (QQ) plot for the
1004 association test shown in (A). This plot is separated by minor allele frequency bin, as indicated by the
1005 colors and shapes of the points. (C) Boxplot showing the distributions of normalized WES-measured
1006 MT-CN in METSIM separated by the number of rs9389268 alternate alleles as detected by imputed
1007 array genotyping (N = 9,791). The EMMAX P value for this variant was 1.62×10^{-8} in imputed data.

1008

1009 **Figure 3. Gene-based associations with MT-CN in WES data.** (A) Manhattan plot and
1010 quantile-quantile (QQ) plot for a gene-based rare variant association test of normalized,
1011 WES-measured MT-CN using WES data from both METSIM and FINRISK (N = 19,034). The red line
1012 represents a Bonferroni significance level of 2.164×10^{-6}, as 23,105 genes were included in this test.
1013 *TMBIM1* is the only gene to reach significance at this level. (B) QQ plot for the test shown in (A). This
1014 plot is separated by minor allele frequency bin, as indicated by the colors and shapes of the points.
1015 (C) Boxplot showing the distributions of normalized WES-measured MT-CN, separated by the number
1016 of WES-detected alternate alleles in *TMBIM1* with MAF < 0.01 and CADD score > 20 (N = 19,034).

1017

1018 **Figure 4. Mendelian randomization approach and results.** (A) Formulation of the Mendelian
1019 Randomization causality test. G represents genotypes, Z is a genetic instrument value constructed
1020 from G, X represents ln(MT-CN), Y represents ln(Insulin), and U represents any confounders of the
1021 association between X and Y. The arrow from X to Y is dashed to indicate that although an association
1022 is known, the relationship is not known to be causal. In this formulation, a significant association
1023 between Z and Y would provide evidence that X is casual for Y. (B) Strategy for choosing variables to
1024 adjust for when building Z in order to enforce MR assumptions. A represents those columns of
1025 covariate matrix W that are associated with Y (represented by the solid line between A and Y) and B
1026 represents those columns of matrix W that are associated with X conditional on A (represented by the
1027 solid line between B and X). Dashed lines represent possible, but unproven associations. The
1028 penalized regression of X on G used to build Z is adjusted for A and B (with no penalty) in an attempt
1029 to prevent any associations between Z and either A or B (represented by the blue X's). While an
1030 association between B and Y is unlikely (represented by the dashed line between B and Y) because B
1031 is not contained in A, B is still adjusted for in the penalized regression to be as conservative as
1032 possible. (C) Strategy for choosing covariates to adjust for in the causality test of Y against Z in
1033 another attempt to reduce the impact of any remaining associations between Z and
1034 assumption-violating variables. Covariate sets I, II, III, and IV are defined by the presence of known
1035 first-order associations (represented by black lines) with Z and Y (see Material and Methods). Yellow
1036 lines represent relationships where a first-order association is not known, but a higher-order
1037 association is possible. Covariate sets II, III, and IV (colored blue) are adjusted for in the causality
1038 test because there is at least one first order association linking them to Z and Y, so they risk violating
1039 MR assumptions 2 or 3. (D) Results of Mendelian randomization test for causality of MT-CN on
1040 fasting serum insulin.

1041 # Tables

1042 **Table 1. Associations of normalized MT-CN with disposition index and Matsuda ISI in METSIM.**

	Disposition index									
	Baseline					Follow-up[b]				
	N	β	SE	P	P*[a]	N	β	SE	P	P*[a]
All subjects	2975	0.094	0.004	3.0×10^{-7}	0.0004	2492	0.062	0.004	0.002	0.068
Excludes diabetic subjects at baseline	2842	0.091	0.003	1.3×10^{-6}	0.0007	2452	0.067	0.004	0.0009	0.041
Excludes diabetic subjects at baseline and during follow-up	2453	0.069	0.003	0.0007	0.023	2449	0.067	0.004	0.0009	0.042
	Matsuda ISI									
	Baseline					**Follow-up[b]**				
	N	**β**	**SE**	**P**	**P*[a]**	**N**	**β**	**SE**	**P**	**P*[a]**
All subjects	2975	0.192	0.005	4.3×10^{-26}	7.3×10^{-17}	2492	0.157	0.006	3.7×10^{-15}	8.7×10^{-10}
Excludes diabetic subjects at baseline	2842	0.191	0.005	1.0×10^{-24}	2.4×10^{-16}	2452	0.161	0.006	1.3×10^{-15}	3.0×10^{-10}
Excludes diabetic subjects at baseline and during follow-up	2453	0.173	0.005	7.2×10^{-18}	5.3×10^{-12}	2449	0.16	0.006	1.7×10^{-15}	3.8×10^{-10}

1043 Testing was done by linear regression using disposition and Matsuda ISI, respectively, as the dependent variable.

1044 [a]P* columns represent the P value from linear regression with additional adjustment for fat mass.

1045 [b]Follow-up measurements were taken at a later time point.

1046

1047

1048 **Table 2. GREML heritability estimates in each cohort separately and in joint analysis.**

		WGS-measured MT-CN			WES-measured MT-CN		
		N[a]	h^2	SE	N[a]	h^2	SE
Joint Analysis	WGS genotypes	4149	0.17	0.06	3916	0.11	0.06
	Imputed genotypes	3916	0.16	0.06	17718	0.09	0.02
METSIM	WGS genotypes	3065	0.31	0.07	2974	0.20	0.08
	Imputed genotypes	2974	0.27	0.08	9791	0.11	0.03
FINRISK	WGS genotypes	1084	0.20	0.22	942	0.24	0.27
	Imputed genotypes	942	0.35	0.27	7927	0.08	0.03

1049 [a]All analyses in this table were limited to sample sets with available imputed genotype data, yielding slightly lower sample
1050 sizes than in other tables.
1051

1052 **Table 3. GREML and GREML-LDMS heritability estimates for normalized MT-CN and**
1053 **low-density lipoprotein (LDL).**

Trait	Genotype source (phenotype source)	N[a]	GREML		GREML-LDMS[b]	
			h^2	SE	h^2	SE
Normalized MT-CN	WGS (WGS-measured MT-CN)	3065	0.31	0.07	0.31	0.09
	Imputed array[c] (WES-measured MT-CN)	6789	0.11	0.04	0.14	0.05
LDL	WGS	3062	0.34	0.08	0.38	0.10
	Imputed array[c]	6787	0.25	0.04	0.32	0.05

1054 [a]All analyses are limited to METSIM data
1055 [b]GREML-LDMS heritability estimates are calculated using PCs 1-10 as fixed-effect covariates.
1056 [c]Analyses of imputed array data exclude samples with WGS data

1057 **Table 4. Single marker association results for rs2288464 and rs9389268**

		FINRISK[a]				METSIM				Joint Analysis			
		N	MAF	P[b]	Beta	N	MAF	P[b]	Beta	N	MAF	P[b]	Beta
rs2288464	Imputed	7927	0.148	0.613	0.0113	9791	0.165	*2.55×10^{-9}*	0.119	17718	0.158	9.77×10^{-7}	0.075
	WES	9221	0.150	0.376	0.0186	9813	0.166	*6.75×10^{-9}*	0.118	19034	0.158	9.34×10^{-7}	0.0734
	WGS	1084	0.142	0.383	0.0532	3065	0.161	0.113	0.0561	4149	0.156	0.0655	0.0562
rs9389268	Imputed	7927	0.354	0.189	0.0216	9791	0.347	*1.26×10^{-10}*	0.0973	17718	0.35	*1.62×10^{-8}*	0.0634
	WGS	1084	0.351	0.788	0.0121	3065	0.347	*3.24×10^{-8}*	0.150	4149	0.348	7.87×10^{-7}	0.115

1058 [a]Analyses of imputed FINRISK array data were performed with covariates for FINRISK genotyping batch.

1059 [b]Italicized results are significant at the appropriate threshold for the given test (see Material and Methods).

1060

1061 **Table 5. Gene-based rare variant association results for *TMBIM1***

	FINRISK			METSIM			Joint Analysis		
	N	Fraction with rare allele	P	N	Fraction with rare allele	P[a]	N	Fraction with rare allele	P[a]
WES	9221	0.016	1.57×10^{-3}	9813	0.013	*1.44×10^{-6}*	19034	0.014	*2.96×10^{-8}*
WGS	1084	0.028	0.489	3065	0.014	0.01	4149	0.013	0.01

1062 *TMBIM1* was the only genome-wide significant gene in the WES rare-variant association tests of METSIM and the whole

1063 dataset.

1064 [a]Italicized results are significant at the appropriate threshold for the given test (see Material and Methods).

1065

1066

1067 **Table 6. Association results between blood cell count traits and MT-CN polygenic risk score in**

1068 **357,656 UK Biobank samples.**

Cell Type	All samples			No *post hoc* high leverage outliers		
	β[a]	SE	P[b]	β[a]	SE	P[b]
Leukocyte	-0.00856	0.00170	*4.42×10^{-7}*	-	-	-
Monocyte	-0.00119	0.00170	0.482	-	-	-
Lymphocyte	-0.00250	0.00170	0.142	-	-	-
Neutrophil	-0.00954	0.00169	*1.80×10^{-8}*	-0.00948	0.00169	*2.17×10^{-8}*
Platelet	0.00548	0.00170	*1.24×10^{-3}*	0.00548	0.00170	*1.25×10^{-3}*

1069 [a]β refers to the regression coefficient of MT-CN in a linear regression of cell type onto MT-CN PRS and other covariates

1070 (see Material and Methods)

1071 [b]P values below a nominal α = 0.05 are shown in italics

1072

1073 **Table 7. Association results between metabolic syndrome traits and MT-CN polygenic risk**

1074 **score in 357,656 UK Biobank samples.**

Trait	Without platelet and neutrophil adjustment			With platelet and neutrophil adjustment		
	β[b]	SE	P[c]	β[b]	SE	P[c]
Type 2 Diabetes	-0.1681	0.0826	*0.0419*	-0.1467	0.0844	0.0823
BMI	-0.0372	0.0175	*0.0331*	-0.0233	0.0175	0.1836
Fat Mass	-0.0452	0.0176	*0.0100*	-0.0318	0.0177	0.0716
C-Reactive Protein	-0.0015	0.0178	0.9305	0.0206	0.0171	0.2291
HDL	0.0573	0.0187	*0.0021*	0.0416	0.0187	*0.0262*
Total Triglycerides	-0.0500	0.0176	*0.0046*	-0.0330	0.0175	0.0603
Weight[a]	-0.0359	0.0176	*0.0414*	-0.0218	0.0178	0.2189

1075 [a]The weight phenotype tested was that which was measured at the time of impedance measurement.

1076 [b]β refers to the regression coefficient of MT-CN in a linear regression of cell type onto MT-CN PRS and other covariates

1077 (see Material and Methods)

1078 [c]P values below a nominal α = 0.05 are shown in italics

Figure 1

A

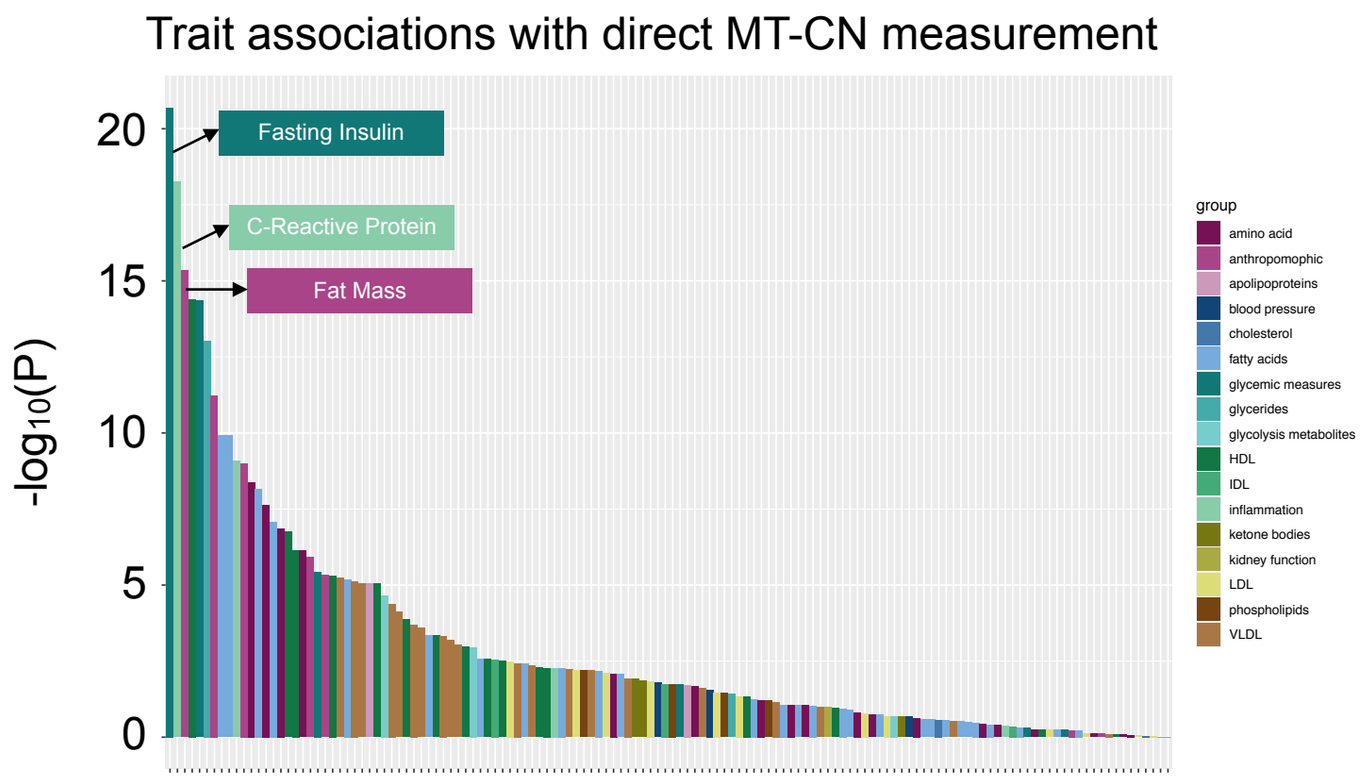

B

Trait	EMMAX model		Conditional on mitochondrial haplogroup	
	P	Beta	P	Beta
Fat mass	4.48×10^{-16}	-0.137	$< 2 \times 10^{-16}$	-0.171
ln(Fasting insulin)	2.02×10^{-21}	-0.182	$< 2 \times 10^{-16}$	-0.226

Figure 2

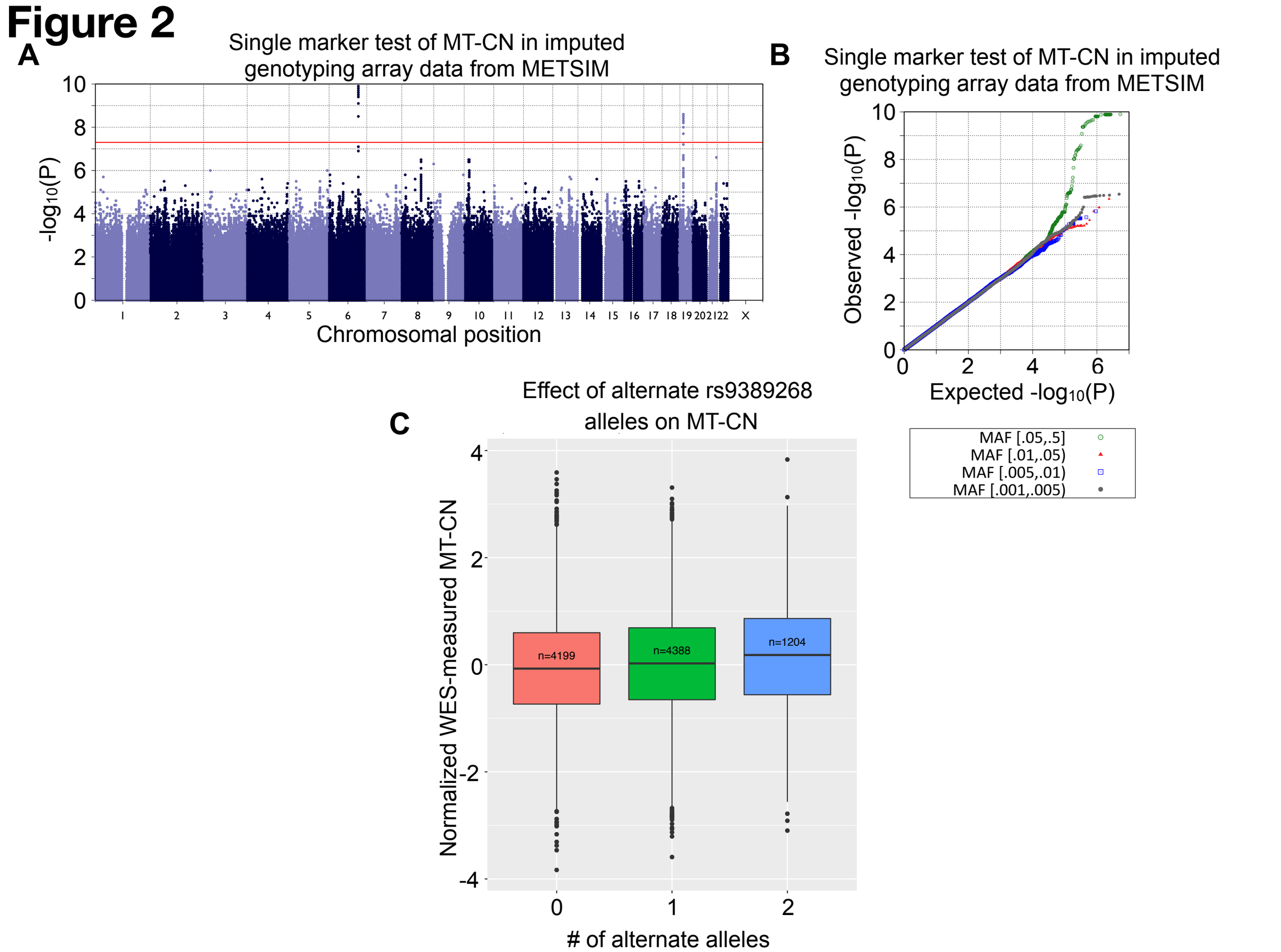
A
Single marker test of MT-CN in imputed genotyping array data from METSIM
-log10(P)
Chromosomal position
B
Single marker test of MT-CN in imputed genotyping array data from METSIM
Observed -log10(P)
Expected -log10(P)
C
Effect of alternate rs9389268 alleles on MT-CN
Normalized WES-measured MT-CN
# of alternate alleles
n=4199
n=4388
n=1204
MAF [.05,.5]
MAF [.01,.05)
MAF [.005,.01)
MAF [.001,.005)

Figure 3

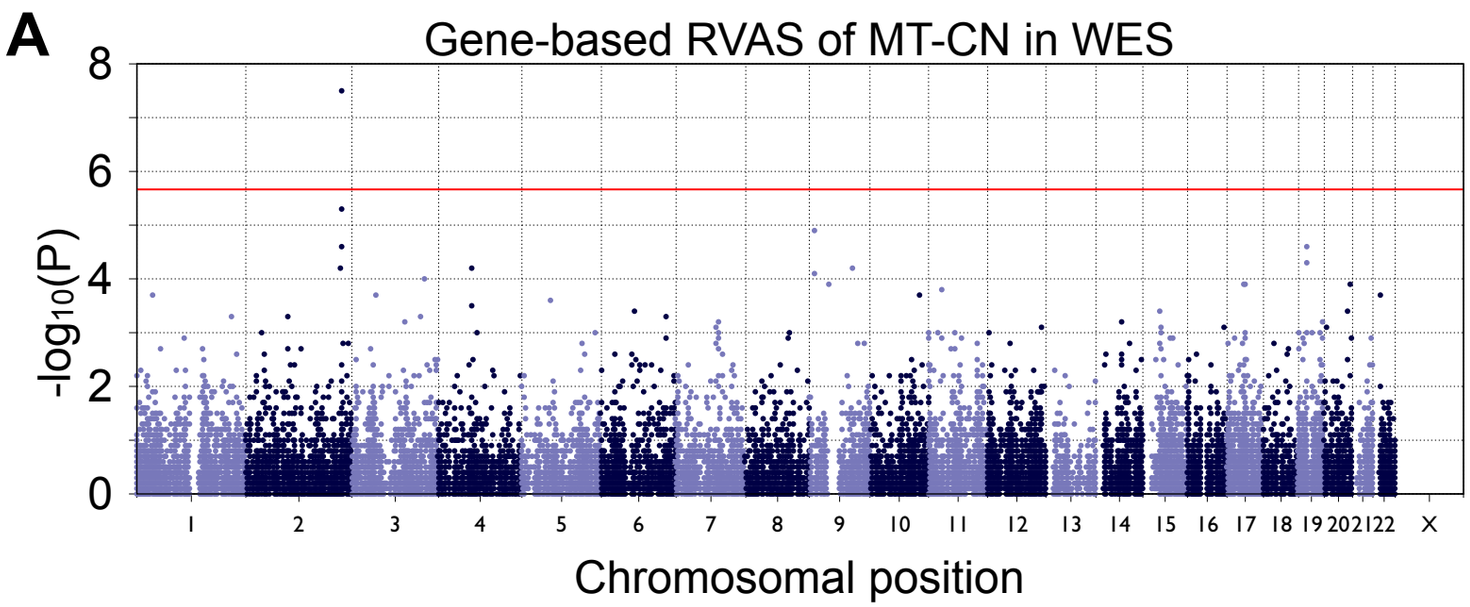
A
Gene-based RVAS of MT-CN in WES
-log10(P)
8
6
4
2
0
1 2 3 4 5 6 7 8 9 10 11 12 13 14 15 16 17 18 19 20 21 22 X
Chromosomal position

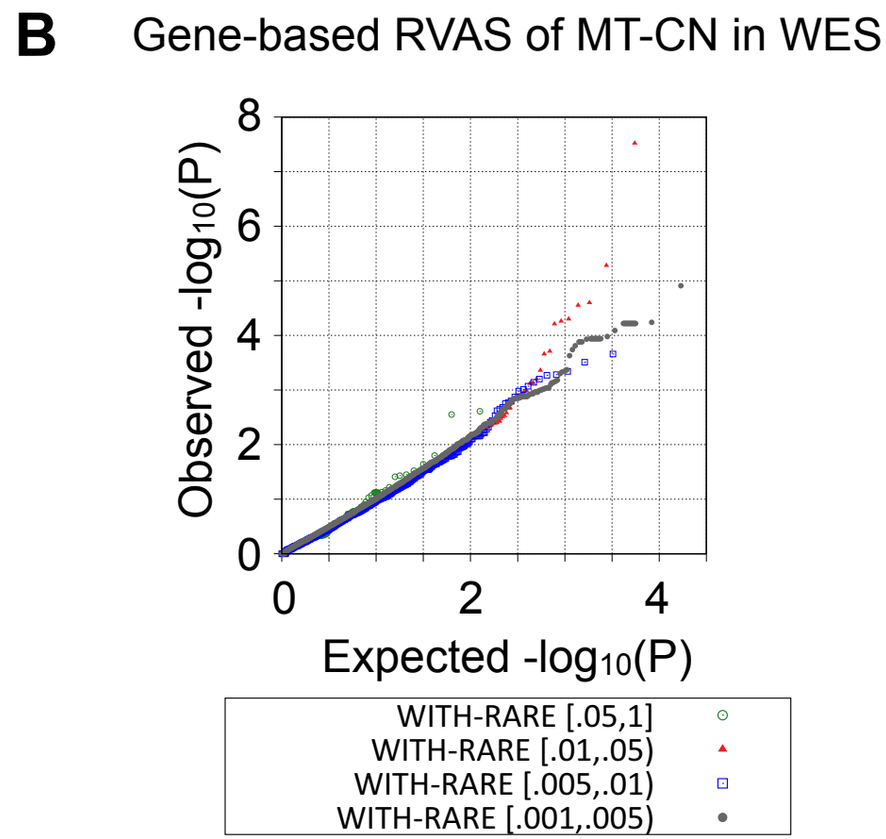
B
Gene-based RVAS of MT-CN in WES
Observed -log10(P)
8
6
4
2
0
0
2
4
Expected -log10(P)
WITH-RARE [.05,1]
WITH-RARE [.01,.05)
WITH-RARE [.005,.01)
WITH-RARE [.001,.005)

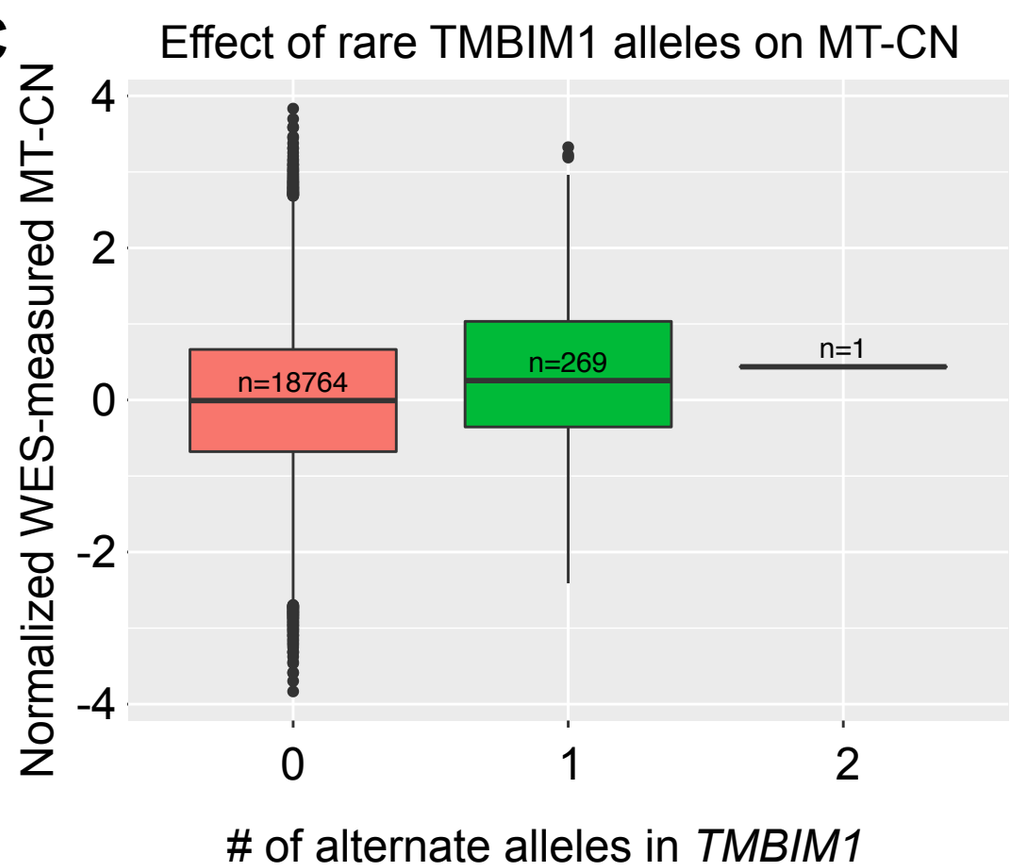
C
Effect of rare TMBIM1 alleles on MT-CN
Normalized WES-measured MT-CN
4
2
0
-2
-4
n=18764
n=269
n=1
0
1
2
# of alternate alleles in TMBIM1

Figure 4

A

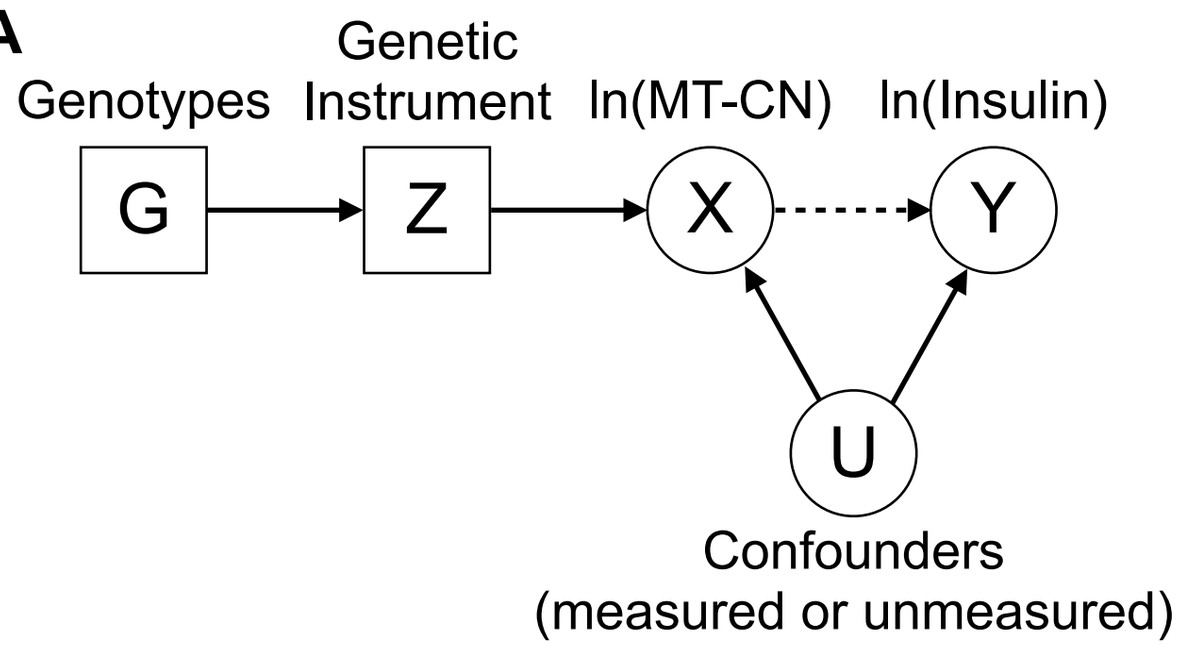

B

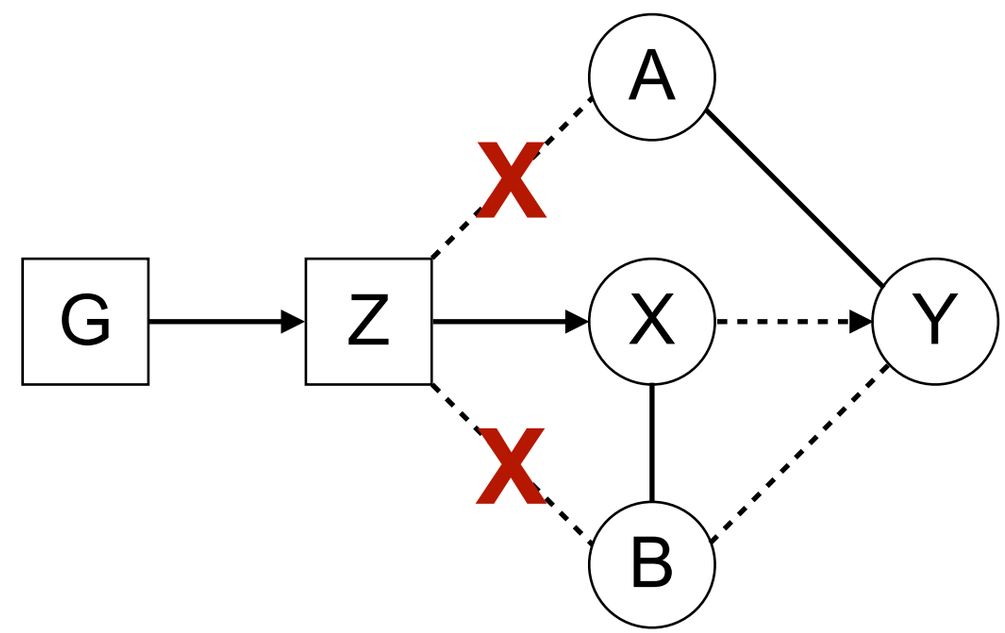

C

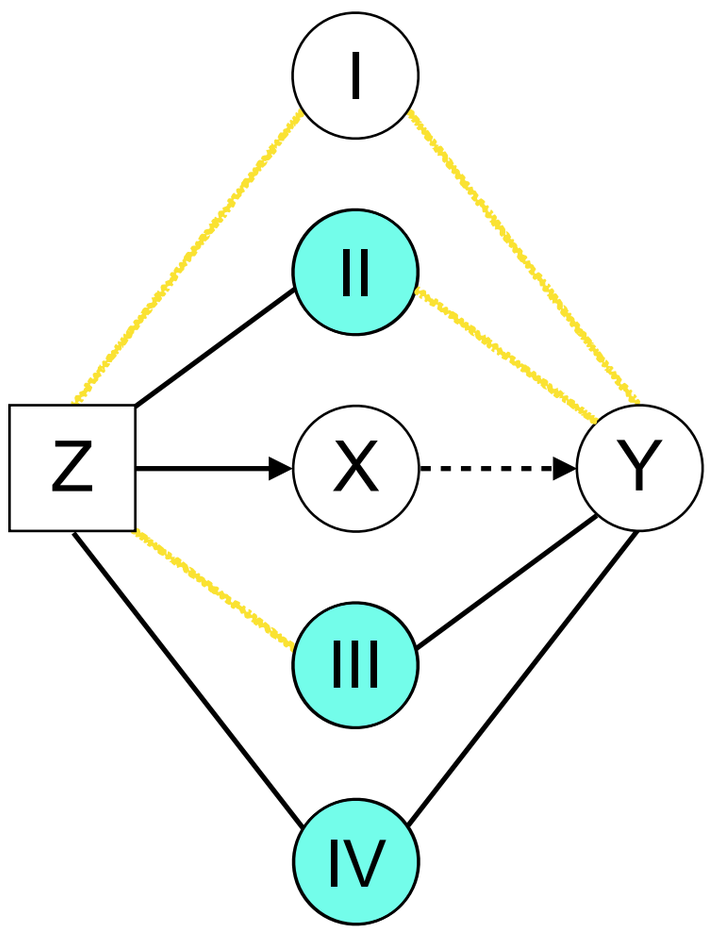

D

Dataset	N	Penalty	Beta	SE	P
WGS	3034	L1	-0.021	0.0131	0.1087
		L2	-0.0212	0.0115	0.0645
Imputed Array	6774	L1	-0.0194	0.0083	0.0192
		L2	-0.0231	0.0079	0.0037
Meta-analysis	-	L1	-0.0199	0.007	0.0045
		L2	-0.0225	0.0065	0.0006